UNIVERSIDAD DE GUANAJUATO

DIVISIÓN DE CIENCIAS E INGENIERÍAS
CAMPUS LEÓN

"ESTUDIO DE LA GENERACIÓN DE ESTEREOCILIOS EN PRECURSORES DE LAS CÉLULAS CILIADAS"

TESIS PROFESIONAL

QUE PARA OBTENER EL TÍTULO DE:
MAESTRA EN CIENCIAS APLICADAS

PRESENTA:

LIC. KAREN CASTAÑO GONZÁLEZ

ASESOR:
DR. VÍCTOR HUGO HERNÁNDEZ GONZÁLEZ

CO-ASESORA:
DRA. VALERIA PIAZZA

LEÓN, GUANAJUATO **MARZO 2020**

ACKNOWLEDGMENTS

First, I would like to thank my advisors, Dr. Víctor Hugo Hernández González and Dr. Valeria Piazza for their support and guidance through this work.

I would also like to acknowledge my evaluation committee for the time spent in reviewing and evaluating the project:

- Dra. Laura Edith Castellano Torres
- Dr. Arturo González Vega
- Dra. Silvia Alejandra López Juárez
- Dr. Luis Carlos Padierna García

I gratefully acknowledge the funding sources from Consejo Nacional de Ciencia y Tecnología (**CONACyT**) for the master studies scholarship and the United States Air Force Office of Scientific Research for the federal grant: **FA9550-17-1-0004**. Also, for the financing granted by Secretaría de Innovación, Ciencia y Educación Superior (SICES) for my master's program: Maestría en Ciencias Aplicadas, through the agreement: **PNPC/SICES/CONV/190/2019UG**

I must express my very profound gratitude to MSc. Ricardo Nieto Fuentes for his assistance and guidance (and patience) on the computing part of this work. Thank you for encouraging me along the way!

I am also grateful to my parents and sister who have provided me through moral and emotional support throughout my years of study and through this process called life.

Additionally, I would also like to thank my friends from the Biophotonics lab. Spending time together and working by your side in the laboratory has been memorable.

Finally, I should thank F.D. Clio N. Bardales Castaño for the assistance modifying some images from the Introduction.

ABSTRACT

Sensorineural deafness is the loss of hearing due to damage to the inner ear caused by some drugs, exposure to very loud sounds or due to genetic mutations. Particularly in mammals, the damage of the hair cells (HC) can be permanent since these cells do not regenerate. For this reason, the study of HC development is important to propose cell replacement therapies. Research on stem cells has given the opportunity to develop auditory cell progenitors. The immortalized multipotent otic progenitor cell line (iMOP), obtained from murine cochlear progenitors, has the capacity for self-renewal and forms spheres (otospheres) that express marker genes of the developing inner ear and the nervous system.

Adenosine triphosphate (ATP) is an important nucleotide involved in purinergic signaling in the hearing organ since the prehearing phase of cochlear development for the maturation and maintenance of hair cells. Studies in multipotent stem cells (MpSC) have concluded that extracellular ATP modulates *in vivo* proliferation, migration, and differentiation; however, the purinoceptors mediating this signaling remain uncharacterized in otic progenitors. The aim of this work was to determine if there is a purinergic pathway, particularly of P2 receptors which is most highly specific for ATP signaling, in iMOP cell line.

The results show that iMOP cells were able to manage different calcium concentrations but showed size variation when applying ATP at different concentrations. Also, ATP concentration-dependent fluorescence intensity variations in iMOP otospheres in the presence of the calcium indicator Fluo-4 and absence of extracellular calcium was observed. This behavior indicates the existence of purinergic P2 receptors in these multipotent otic progenitors. According to the response's patterns, three main trends were found which were classified into positive or negative response. Furthermore, there was a decrease of intracellular calcium in the presence of the P2-purinoceptor antagonist suramin, confirming for the first time the presence of ATP receptors in the iMOP cell line. A spectral analysis in which time domain was transformed into frequency domain was also performed on the calcium signaling data. This analysis suggests that there is a relationship between ATP concentration and the frequency range response. In addition to the contribution to purinergic signaling research in this work, an interactive open-access program which allows a frame-by-frame analysis of regions of interest was created.

RESUMEN

La sordera neurosensorial es la pérdida de la audición por daño en el oído interno causada por el uso de algunos fármacos, exposición a sonidos muy altos o debido a mutaciones genéticas. Particularmente, el daño de las células ciliadas puede ser permanente ya que estas células no se regeneran. Por tal motivo, el estudio de su desarrollo y de la formación de sus estereocilios es importante para plantear terapias de reemplazo celular. La investigación sobre células troncales ha dado la oportunidad de desarrollar progenitores de células auditivas. La línea celular iMOP (immortalized multipotent otic progenitor cells), se obtuvo a partir de progenitores cocleares murinos, tiene la capacidad de autorrenovarse y formar esferas que expresan genes marcadores del oído interno en desarrollo y del sistema nervioso.

El ATP es un nucleótido importante en la señalización purinérgica del órgano auditivo desde el periodo previo a la escucha durante el desarrollo coclear y para la maduración y mantenimiento de las células ciliadas. Estudios en células madre multipotentes (MpSC) han concluido que el ATP extracelular modula la proliferación, migración y diferenciación *in vivo*, sin embargo, los purinoceptores que median esta señalización no ha sido caracterizados en progenitores óticos. El objetivo del presente trabajo fue determinar la existencia de una vía purinérgica, particularmente de receptores P2, que es específica para la señalización de ATP en la línea celular iMOP.

Los resultados muestran que las células iMOP pudieron manejar diferentes concentraciones de calcio, pero además, mostraron una variación de tamaño al aplicar ATP a diferentes concentraciones. También se observaron variaciones de la intensidad de fluorescencia dependientes de la concentración de ATP, en presencia del indicador de calcio Fluo-4 y ausencia de calcio extracelular, en otoesferas de células iMOP. Este comportamiento indica la existencia de receptores purinérgicos P2 en dichos progenitores óticos multipotentes. De acuerdo con los patrones de respuesta, se encontraron tres tipos de comportamiento principales que a su vez se clasificaron en respuestas positivas o negativas. Además, se observó una disminución del calcio intracelular en presencia de suramina, antagonista del purinoreceptor P2, confirmando por primera vez la presencia de receptores de ATP en la línea celular iMOP. También se realizó un análisis espectral en el que los datos de señalización de calcio del dominio del tiempo se transformaron al dominio de frecuencia. Este análisis sugiere la existencia de una relación entre la concentración de ATP y la respuesta en un rango de frecuencia. Además de la contribución a

la investigación de señalización purinérgica, en este trabajo se obtuvo un programa interactivo de acceso libre que permite un análisis de imagen por imagen de regiones de interés.

INDEX

1. Introduction 1

1.1 The cochlea 1

1.2 Development of the mammalian cochlea 5

1.3 Calcium signaling in the auditory system 11

1.4 iMOP cells 14

1.5 Microscopy & Cell calcium imaging 16

1.5.1 Fluorescence microscopy 16

1.5.2 Fluo-4 17

1.5.3 Laser scanning confocal microscopy 18

2. Statement 20

3. Aims 20

4. Materials and methods 21

4.1 Cell culture 21

4.1.1 Maintaining, freezing and thawing iMOP cells 21

4.1.2 Differentiating iMOP cells into Sensory Epithelium 22

4.1.3 Differentiating iMOP cells into Neurons 22

4.1.4 Fixing, staining and mounting iMOP cells 23

4.2 Calcium imaging 24

5. Results 32

5.1 Confocal Microscopy 32

5.2 Calcium Imaging 34

6. Discussion and Conclusions 48

References 52

FIGURE INDEX

FIGURE 1. STRUCTURE OF THE HUMAN EAR. 2

FIGURE 2. ANATOMY OF THE COCHLEA. 3

FIGURE 3. STEREOCILIARY BUNDLES. 4

FIGURE 4. HAIR CELLS MECHANOELECTRICAL TRANSDUCTION. 4

FIGURE 5. DEVELOPMENT OF THE INNER EAR. 6

FIGURE 6. STRUCTURE OF THE ORGAN OF CORTI SHOWN IN CROSS-SECTION. 7

FIGURE 7. IMMATURE ORGAN OF CORTI IN A POSTNATAL PRE-HEARING RAT COCHLEA, SHOWN IN CROSS-SECTION. 8

FIGURE 8. PURINERGIC RECEPTORS AND THEIR NATURAL LIGANDS. 12

FIGURE 9. CA^{2+} SIGNALING IN THE INNER EAR. 13

FIGURE 10. IMOP CELLS. HOECHST STAIN LABELS NUCLEI AND ANTIBODY LABELING REVEALS SOX2 AND C-MYC. 15

FIGURE 11. SKELETAL FORMULAS OF FLUO-4. 17

FIGURE 12 LASER SCANNING CONFOCAL MICROSCOPE OPTICAL CONFIGURATION. 18

FIGURE 13. CONFOCAL AND WIDEFIELD FLUORESCENCE MICROSCOPY. 19

FIGURE 14. FLOWCHART SUMMARIZING THE SECTION 4.2 OF THE MATERIALS AND METHODS CHAPTER. 25

FIGURE 15. 35 MM DRILLED CULTURE DISHES READY TO USE FOR CALCIUM IMAGING ACQUISITION. 26

FIGURE 16. VIDEO FRAMES EXTRACTED FROM A TIME SEQUENCE OF AN EXPERIMENT. 28

FIGURE 17. REPRESENTATIVE FLUORESCENCE INTENSITY VARIATIONS ANALYSIS. 29

FIGURE 18. ANALYSIS PROGRAM GRAPHICAL EXAMPLE. 30

FIGURE 19. PHASE CONTRAST IMAGES OF OTOSPHERES. 32

FIGURE 20. IMOP CELLS CULTURES CONFOCAL MICROGRAPHS. 33

FIGURE 21. MICROGRAPHS OF IMOP CELLS AFTER 60 MIN UNDER DIFFERENT CA^{2+} CONCENTRATIONS. 34

FIGURE 22. NOTCHED BOXPLOT OF IMOP CELLS SIZE CHANGE RATE AFTER ATP STIMULATION AT DIFFERENT CONCENTRATIONS. 35

FIGURE 23. MICROGRAPHS OF IMOP OTOSPHERES EXPOSED TO DMSO. 36

FIGURE 24. REPRESENTATIVE GRAPHS OF FLUORESCENCE INTENSITY VARIATION OVER TIME. 37

FIGURE 25. DOSE-RESPONSE RELATIONSHIP BETWEEN THE DIFFERENT ATP CONCENTRATIONS. 37

FIGURE 26. CLASSIFICATION OF THE DIFFERENT TYPES OF RESPONSE TO ATP. 38

FIGURE 27 INTERCELLULAR CA^{2+} SIGNALING USING FLUO-4 IN IMOP CELLS. 40

FIGURE 28 INTERCELLULAR CA^{2+} SIGNALING USING FLUO-4 IN IMOP CELLS. CONTROLS. 41

FIGURE 29. IMOP CELLS BASELINE TEMPORAL CURVE OF THE RELATIVE FLUORESCENCE INTENSITY CHANGE. 42

FIGURE 30. A SINUSOIDAL FUNCTION G(T) (A) AND A CA^{2+} RECORDING. 43

FIGURE 31. FREQUENCY DISTRIBUTION HISTOGRAMS OF CALCIUM RESPONSES TO ATP. 46

FIGURE 32 FREQUENCY DISTRIBUTION HISTOGRAMS OF CALCIUM RESPONSES TO HBSS AND SURAMIN. 47

1. INTRODUCTION

1.1 THE COCHLEA

The ear is a sensory organ of the human body responsible for two important functions. The most ancient task that has remained essentially the same from the fish to the human being is to maintain our sense of postural equilibrium and coordination of head and eye movements. A more advanced function found in higher vertebrates is to detect, transmit and transduce sound to the brain through the three main parts of the ear: the outer ear, the middle ear and the inner ear [1].

As shown in Figure 1, the **external ear** is comprised of the auricle or pinna, the skin-covered cartilage that is attached to the outside of the head, and the external auditory canal, a narrow passage in the temporal bone closed by the tympanic membrane. The **middle ear** is a small air-filled cavity in the temporal bone connecting the tympanic membrane with the tympanic cavity. The tympanic cavity contains a chain of three tiny bones called the malleus, incus, and stapes, collectively called the auditory ossicles. The **inner ear**, often referred to as the labyrinth (Figure 2 A), is made of a bony structure (bony labyrinth) and its content (membranous labyrinth) and consists of several sensory organs. These are the vestibular system, intended for postural equilibrium formed by the saccule, the utricle and the three semicircular canals; and the cochlea, a tiny coiled structure responsible for hearing [1, 2].

Sound waves are funneled through the external ear and channeled into the external auditory canal causing the eardrum to vibrate. The vibrations enter the middle ear and are transferred to the ossicles, their movement pushes a membrane, called the oval window, in and out of the bony enclosure of the cochlea converting sound waves into fluid waves. In this way, the sound is conducted to the inner ear, where the organ of Corti plays the role of converting sound waves into electrical signals. Dendrites of the spiral ganglion neurons (SGNs) synapse to the hair cells and take the neural signals to the auditory pathways in the brain [3].

The **cochlea** is comprised of three chambers: the scala vestibuli, the scala tympani and the scala media (Figure 2 B). The ionic composition of the fluid in the scala media (endolymph) is like that of intracellular fluid, rich in potassium (K^+) and low in sodium (Na^+). The fluid in the scala vestibuli and the scala tympani (perilymph) resembles the extracellular fluid, and thus rich in Na^+ and poor in K^+ [4]. The lateral wall of the scala media is composed of the outer spiral sulcus, stria vascularis, and spiral ligament. The stria

vascularis is responsible for maintaining the ion composition of the endolymph and producing an endocochlear potential (EP) in the scala media [5]. The endocochlear K^+ concentration and the EP are both indispensable for depolarizing the cochlear hair cells to transduce acoustic stimuli to bioelectrical impulses that are relayed to the spiral ganglion neurons [4, 6].

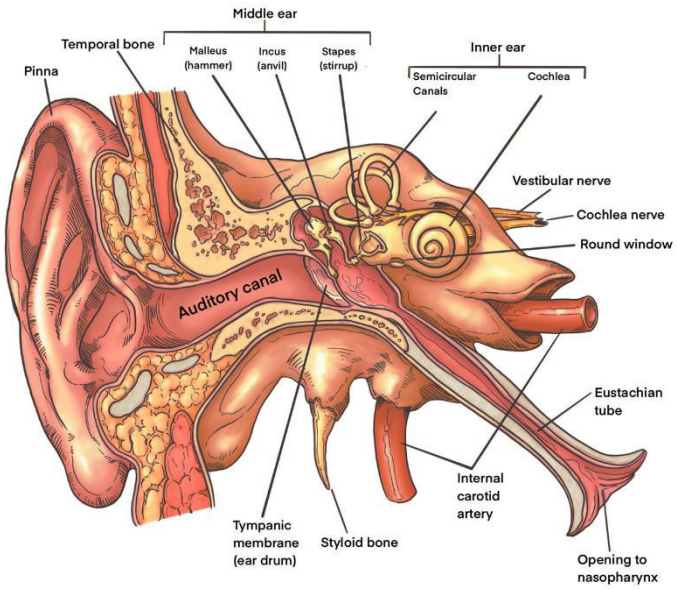

Figure 1. Structure of the human ear. The ear is made up of three distinct parts: the external, middle and inner ear. They all have different, but important, features that facilitate hearing and balance. *From [7]*

The basilar membrane, located between the scala media and the scala tympani, allows the separation of the sound that travels from the base towards the apex of the cochlea according to its specific frequency corresponding to the tonotopic mapping of the cochlea [8]. The **organ of Corti** (Figure 2 *C*) sits on the basilar membrane and contains sensory hair cells and nonsensory supporting cells, both of which are polarized epithelial cells.

Cochlear hair cells consist of two cell types, the **outer hair cells** (OHCs) and the **inner hair cells** (IHCs) arranged as one row of IHCs and between three and five rows of OHCs. Due to a putative molecular motor called prestin, outer hair cells can contract and expand producing amplification of vibrations while inner hair cells oversee the transduction [9]. Both IHCs and OHCs have bundles of stereocilia on their top. Stereocilia are actin-based protrusions with a highly precise geometry that is required to detect nanoscale movements, and they constitute part of the mechanoelectrical transducer. To detect these small movements stereocilia are organized into a bundle with three rows of stereocilia that increase in height in a stair-like fashion (Figure 3) and are connected to one another by different link types [10].

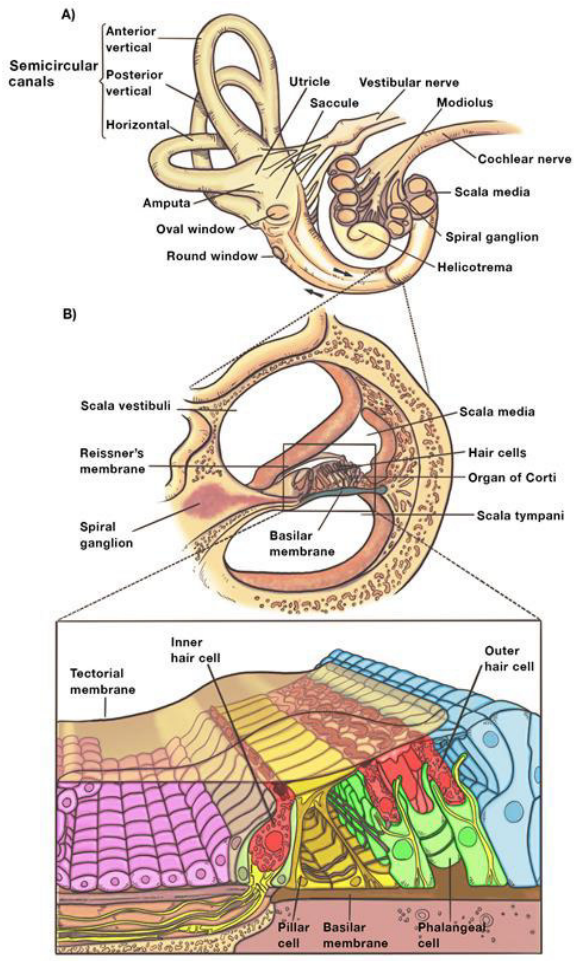

Figure 2. Anatomy of the cochlea. A) The structure of the inner ear, the cochlear spiral shows the fluid-filled tubes of the labyrinth. B) Cross-section of the cochlear spiral showing the arrangement of the three fluid-filled ducts, the location of the basilar membrane and the organ of Corti. C) Cross-section of the organ of Corti, showing the arrangement of the inner and outer hair cells. Adapted from *[8]*

Just like other epithelial cells, the basal and apical surfaces of the HC are separated by tight junctions, allowing separate extracellular ionic environments at these two surfaces. The apical end is exposed to the endolymph, while the basal end is bathed in perilymph [11].

The tectorial membrane (TM), made of collagens and molecules known as tectorins, covers the organ of Corti. It is attached only on one side and is raised above the basilar membrane. Its structure varies along the cochlear axis being narrow and thin at the base, and wider and thicker at the apex [12]. Although it has been difficult to determine, it seems that the tallest tips of the OHCs stereocilia are embedded in the overlying tectorial membrane, whereas the tips of the IHCs stereocilia are not. So, when the basilar membrane moves up and down, a subtle movement occurs between the tectorial membrane and the organ of Corti, resulting in OHCs stereocilia deflection [13].

On the other side, IHCs hair bundle is deflected when the fluid endolymph moves in response to sound. At the resting potential, only a small fraction of the transduction channels is open. When the hair bundle bends (Figure 4), cation-selective transduction channels open allowing K^+ ions to flow into the cell [6, 11]. When the hair bundle is displaced in the direction of the tallest stereocilium, more transduction channels open, causing depolarization as K^+ enters the cell. Depolarization, in turn, opens voltage-gated calcium (Ca^{2+}) channels in the hair cell membrane and the resultant Ca^{2+} influx modulates transmitter (glutamate) release from the afferent synapse in auditory nerve fibers. As the receptor potential is biphasic: movement in the opposite direction leads to hyperpolarization which prevents the influx of K^+ and closes the Ca^{2+} channels resulting in smaller release, or no release of the transmitter. The auditory nerve carries this

electrical signal to the auditory cerebral cortex, which turns it into a sound that we recognize and understand [4, 11].

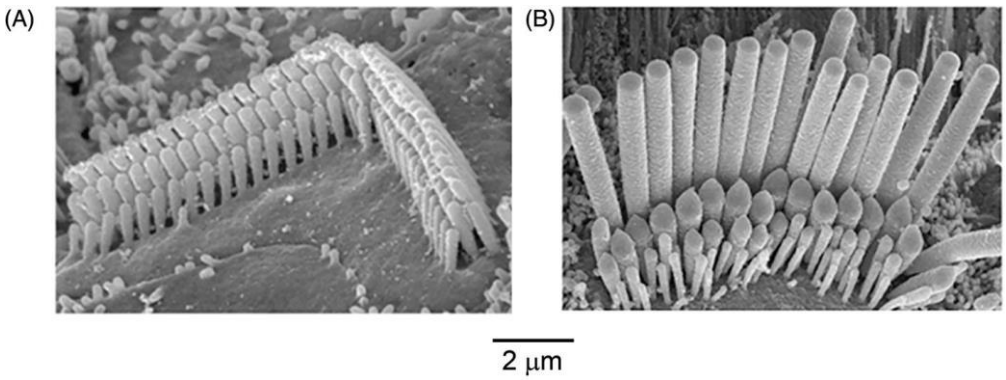

Figure 3. Stereociliary bundles. Scanning electron micrographs of guinea pig's stereociliary bundles showing the staircase in heights of the rows of A) an OHC, where the stereocilia form V- or W-shaped rows and B) an IHC, where the stereocilia form nearly straight rows. Modified from *[14]*

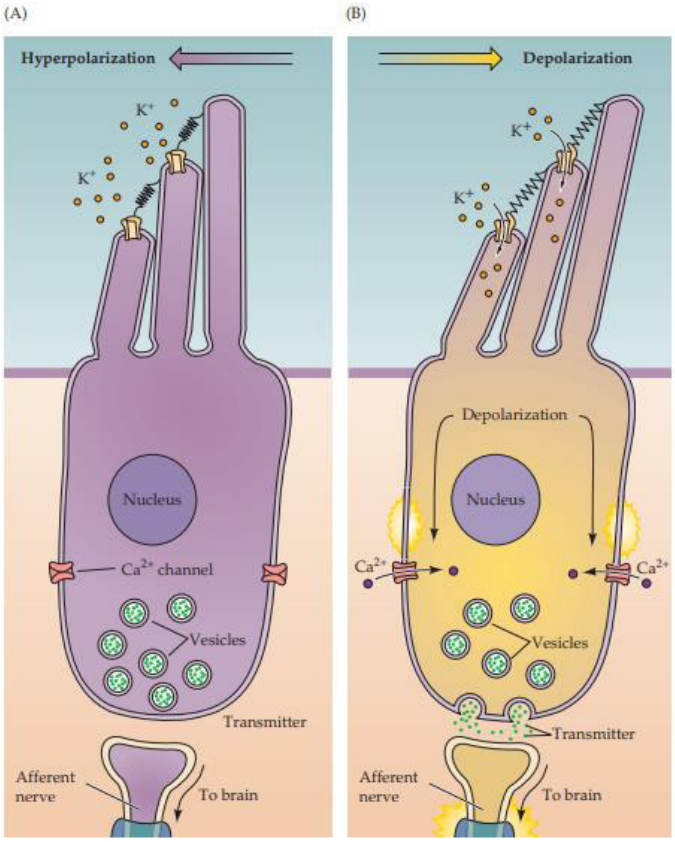

Figure 4. Hair cells mechanoelectrical transduction. A) Deflection of the stereocilia toward the smallest stereocilium, causes transduction channels to close. In this situation, the hair cells become hyperpolarized and the nerve afferents are not excited B) Hair bundle deflection in the opposite direction, opens selective channels near the tips of the stereocilia, allowing K^+ ions to flow into the hair cell causing its depolarization and leading to the excitement of the cochlear nerve afferents. From *[11]*.

1.2 DEVELOPMENT OF THE MAMMALIAN COCHLEA

In mice, the most commonly used model system for the developing mammalian cochlea, the inner ear evolves from a thickening of the ectoderm known as the otic placode, derived from the anterior border of the neural plate called the preplacodal region (Figure 5). Around embryonic day 8 (E8), the otic placode invaginates and pinches off to form a fluid-filled cyst known as the otocyst, which is close to the hindbrain and notochord [15]. After otocyst closure, the inner ear is progressively specified by signals arising from surrounding tissues conferring its positional identity along the anterior–posterior (AP), the dorsal–ventral (DV), and the medial–lateral (ML) axes [16]. AP axis, the first one to be established, specifies the neuro-sensory domain (NSD) in the anterior otocyst. Next, the DV restricts the NSD to the ventral portion of the otocyst. Finally, the ML axis establishes the types of neurons formed within the NSD (vestibular or auditory) [17, 18, 19].

At E11, the endolymphatic duct and sac are derived from the dorsomedial region of the otocyst and the cochlear duct begins its growth at the ventral tip of the elongated otocyst. Cells become specified along the otocyst resulting in sensory patches. Cells within these patches are considered progenitor cells due to their multipotency, the ability to generate hair cells and supporting cells [20]. To avoid cell overpopulation after the specification of the cochlear prosensory domain, regulation of the number of cells is mediated through terminal mitosis beginning at the apex at E12.5 and proceeding gradually toward the base [21]. Around the same time, the SGNs exit the cell cycle in a base to apex progression and seem to aggregate and elongate along with the growing cochlear duct [22, 23]. At the end of the elongation of the cochlear duct, the spiral ganglion is visible in Rosenthal's canal, connected by radial fibers to the developing organ of Corti [24].

On the contrary, cells in the prosensory domain begin differentiation at the base and proceed towards the apex of the cochlea between E14 and E15. The organ of Corti is recognizable at E16 in the nascent basal turn of the cochlear duct and comprises the greater epithelial ridge (also known as Köllicker's organ), and the lesser epithelial ridge separated by a pair of immature inner and outer pillar cells [25] that will lead to the opening of the tunnel of Corti. By E17, mechanosensory hair cells differentiate in the basal turn and use a lateral inhibition mechanism based on notch signaling to prevent neighboring precursor cells from becoming hair cells. Cochlear extension and coiling continue until around E19 or postnatal day 0 (P0), when the duct reaches its mature shape [26]. Unlike healthy humans who can hear at birth, mice are born deaf and acquire hearing around P12 [27].

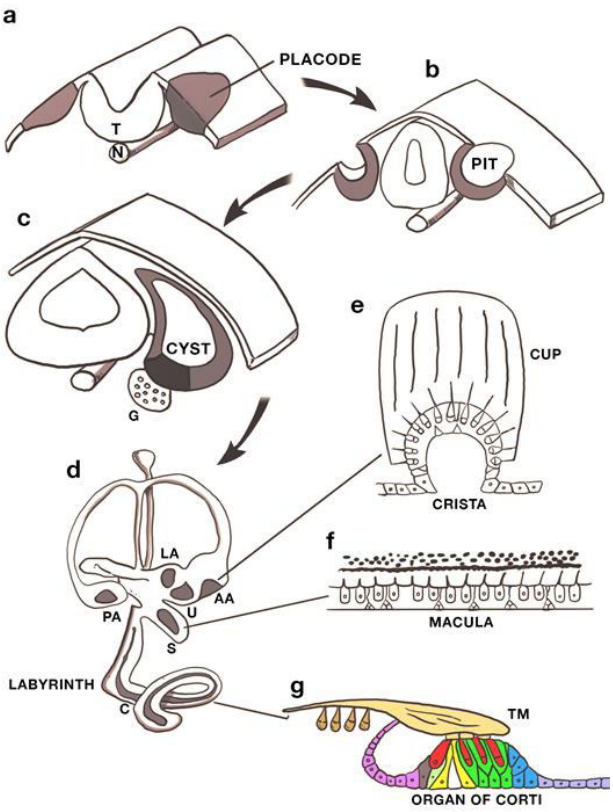

Figure 5. Development of the inner ear. The inner ear develops from the otic placode (a) an ectodermal thickening that invaginates to form the otic pit (b) which in turns pinches off from the ectoderm to form the otic vesicle (c). The different sensory organs are derived from a common pro-sensory patch (black) in the ventromedial wall of the otocyst (c). A complex series of morphogenetic events transforms the otic vesicle (c) into the labyrinth (d) containing three cristae (e), two maculae (f), and an organ of Corti (g). Abbreviations: G, VIIIth ganglion; AA, anterior ampulla; LA, lateral ampulla; PA, posterior ampulla; U, utricle; S, saccule; C, cochlea; CUP, cupula; OM, otoconial membrane; TM, tectorial membrane. From *[28]*

The organ of Corti (OC) (Figure 6) is one of the most precise and sophisticated patterned structures in mammals. It is comprised of four general cell types: sensory neurons, hair cells, supporting cells and general otic epithelium uniquely distributed in and around the OC. Furthermore, it is innervated by ear-derived spiral ganglions afferent neurons and brainstem-derived motor efferent neurons [29]. Each hair cell is surrounded by supporting cells: inner phalangeal and border cells surround the inner hair cells while Deiters' cells surround the outer hair cells. In addition, an inner and outer pillar cell separate these two domains and form the tunnel of Corti. To achieve this precise arrangement along the length of the cochlea, strict control of proliferation and differentiation of hair cells and supporting cells progenitors is necessary [30]. The molecular mechanisms guiding this process are not fully elucidated, yet some genes are shown to be crucial for the process. For the purpose of this work, only few of the molecular mechanisms are briefly mentioned here.

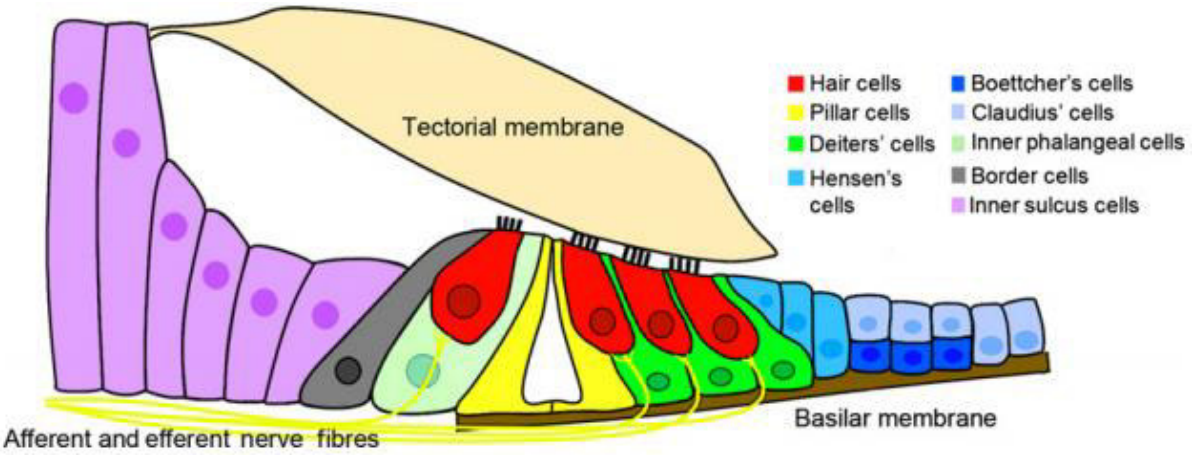

Figure 6. Structure of the organ of Corti shown in cross-section. The organ of Corti consists of epithelial cells that are varied in both structure and function. Cochlear hair cells (red) can be anatomically and functionally divided into inner and outer hair cells. Each hair cell is surrounded by dedicated kinds of supporting cells (light green, gray and green). In addition, an inner and outer pillar cell (yellow) separate these two domains and form the tunnel of Corti (white area between the pillar cells). The tectorial membrane is an acellular sheet secreted largely by the inner sulcus cells (light purple) in the greater epithelial ridge. From *[30]*

Although the precise origin of cochlear duct progenitors is still unknown, by embryonic day 11, the ventral portion of the mouse otocyst contains four gene expression domains, which will transform into the main divisions of the cochlear duct as it grows out from the ventral otocyst [31]. The ventromedial region expresses a domain of Sox2 and Jag1, where cells are hypothesized to be multipotent and can give rise to the prosensory domain [32, 33, 34]. Kölliker's organ (Figure 7) derives from the antero-ventral region of the otocyst, which overlaps somewhat with Sox2 expression and expresses Lunatic fringe gene (Lfng) and fibroblast growth factor 10 (Fgf10) [34, 35, 36]. Adjacent to the Sox2/Jag1+ domain, on the abneural side of the cochlea, is a narrow strip of non-sensory cells that express Bmp4 [37]. As development progresses, the Bmp4+ region expands, upregulating markers of the future outer sulcus and downregulating marker genes of Kölliker's organ. The central, prosensory domain gives rise to the organ of Corti [26, 38], and is surrounded by two nonsensory domains. The domain closest to the auditory ganglion, the neural side namely Kölliker's organ, develops into the inner sulcus, whereas the domain on the opposite, abneural side of the prosensory domain develops into the outer sulcus [34].

Then, around E13.5, the cyclin-dependent kinase inhibitor p27kip1 (Cdkn1b) is upregulated in an apical-to-basal gradient that closely follows the gradient of cell cycle exit [39]. Together, cyclin-dependent kinase inhibitors and some members of the pocket protein family (Rb1, Rbl1/p107, Rbl2/p130) have been reported to be necessary after cell cycle exit to maintain the post-mitotic state and viability of both hair cells and supporting cells [40, 41].

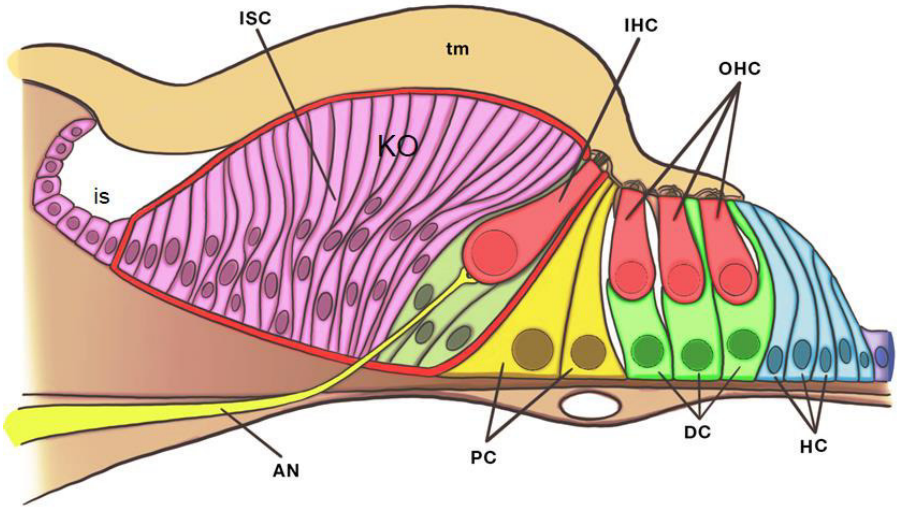

Figure 7. Immature organ of Corti in a postnatal pre-hearing rat cochlea, shown in cross-section. Kölliker's organ (or greater epithelial ridge) is a transient structure consisting of columnar-shaped supporting cells that will become the inner sulcus region by the onset of hearing (P11-13). *AN* auditory nerve, *DC* Deiters' cell, *HC* Hensen's cell, *IHC* inner hair cell, *is* inner sulcus, *ISC* inner supporting cell, *KO* Kölliker's organ (outlined in red), *OHC* outer hair cell, *PC* pillar cell, *tm* tectorial membrane. Modified from *[42]*.

After mitotic arrest, a signaling pathway considered to be playing a role in prosensory formation is the fibroblast growth factor (FGF) pathway that is possibly required for one of the key events for hair cells (HC) development: the expression of Atoh1 [26]. Atoh1 is thought to be the earliest determinant of HC fate [43, 44]. Furthermore, the interaction of proliferation genes such as the Mycs with differentiation genes such as Atoh1 and possibly other upstream genes is needed in the development of hair cells [45].

Different signaling pathways, transcription factors expression and epigenetic regulations are required for hair and supporting cells specification. Furthermore, cells are usually exposed to more than one stimulus at a time, and crosstalk between signaling pathways is evident and has been identified.

Sox2

Sox2 protein (SRY-related HMG box) is a high-mobility group related transcription factor. It is known to regulate self-renewal and maintenance of stem cells and is expressed by neural progenitors at different stages of development [46, 47]. In the inner ear, Sox2 is one of the earliest markers in the otic progenitor cells that will develop as both the prosensory and neuronal cell lineages [33, 48]. Sensory patches co-express the Notch ligand Jag1 and Sox2, therefore, it has been suggested that Sox2 expression itself is dependent on Notch signaling [49, 50]. A subset of Sox2+ cells first express the prosensory transcription factor Atoh1 around E13.5, when the prosensory cells have become postmitotic, then the cells mature and Sox2 is downregulated until it is undetectable in the early

postnatal period. While adjacent supporting cells maintain Sox2 expression, Sox2 expression reduction is crucial for hair cell maturation as Sox2 antagonizes Atoh1. [51, 52].

FGF signaling

The Fibroblast Growth Factor (FGF) gene family is among the prime candidates to control inner ear induction since it has several stage-specific functions during inner ear development. At early stages (E9-E10), FGF signaling is important for the specification of the otic domain [53]. FGF3 and FGF10 signal to the overlying ectoderm induce the formation of the otic placode and vesicle [54]. FGF10 is expressed in all vestibular sensory patches and is necessary for their development [55, 56] but it is also a potential candidate for cochlear prosensory designation [30]. FGF20 is expressed in the prosensory region of the cochlea overlapping Sox2 expression [57, 58] and after E15 it regulates differentiation of outer hair cells (OHC) and supporting cells (SC) in the organ of Corti [58]. FGF9 expressed in the non-sensory epithelium, and FGF20, expressed in the sensory epithelium, regulate the number of cochlear progenitors and the ultimate length of the cochlea through signaling to mesenchymal FGF receptors (FGFRs) [58].

BMP signaling

Bone Morphogenetic Proteins (BMPs) are secreted signaling molecules that belong to the transforming growth factor-beta (TGFβ) family of growth and differentiation factors. BMP signaling is an important step in patterning the cochlea across its abneural–neural axis. Intermediate levels of BMP signals are responsible for the specification of prosensory fates, whereas low doses specify Kölliker's organ and high doses generate outer sulcus and inhibit Kölliker's organ gene expression [34]. Particularly, Bmp4 is one of the early proteins asymmetrically expressed as the cochlear duct begins to grow [34] and has been reported as necessary for the patterning of the sensory and non-sensory portions of each crista ampullaris at the base of the mammalian semicircular canals [35, 59]. Nevertheless, Bmp4 expression suggests that it could play a pivotal role in the specification of the cochlear prosensory domain [59].

Notch-Jagged signaling

Notch signaling is an evolutionarily conserved pathway that affects cell differentiation decisions across a broad range of cell types in a single organism and at different steps during cell lineage progression [60]. It mediates several critical events during inner ear development, including determining the hair and supporting cells; and neuronal and non-neuronal cell fate choices through lateral inhibition [61].

The Notch ligand Jagged1 is expressed in all sensory patches in the inner ear together with Sox2 [62, 63]. However, in the mammalian cochlea, Jag1 protein expression is quickly restricted to the non-sensory domain on the neural side of the cochlea and is not co-expressed with markers of the prosensory domain [34]. This suggests that Jag1-Notch is necessary for the induction of the vestibular organs but is not necessary for the induction of the cochlear prosensory domain, from which Jag1 is excluded by the time the first specific prosensory markers are induced [32, 64].

Atoh1

The basic helix-loop-helix (bHLH) transcription factor Atonal homolog1 (Atoh1 or Math1) is one of the earliest markers to be expressed in differentiating hair cells [43, 65]. Starting between E13.5 and E14.5, Atoh1 is upregulated in nascent hair cells in the mid-basal region of the cochlea, and spreads apically along the prosensory domain until patterning is complete around E17.5. Atoh1 is subsequently downregulated, starting at about E17.5 and reduced to barely detectable levels by post-natal day 6 (P6) [66]. Wnt proteins and BMPs have been shown to regulate Atoh1 hair cell production in the cochlea [67, 68, 69]. The regulation of Atoh1 expression by the Notch signaling pathway in the inner ear is also well documented. Besides its role in early hair cells specification, Atoh1 is also important later during development by promoting their survival and maturation [65, 70].

1.3 CALCIUM SIGNALING IN THE AUDITORY SYSTEM

Sensory systems refinement during development rely on periods of experience-independent action potential activity before the onset of function to guide the maturation of circuits required for processing sensory information [71, 72]. In all sensory modalities examined, this spontaneous activity occurs in the form of discrete bursts of electrical activity separated by long periods of quiescence [72, 73] that promote maturation and survival of sensory neurons, refinement of neuronal connections in the central nervous system, and assembly of appropriate functional networks [74]. In the auditory system, spontaneous electrical activity that is present before the onset of hearing (defined as the age range over which auditory neurons reliably respond to sound-evoked stimulation, around P11-13 in mouse [27, 75]) has also been involved in shaping the organization of nascent circuits [76]. Increases in cytoplasmic intracellular calcium concentrations $[Ca^{2+}]_i$ which propagate from cell to cell are known as intercellular Ca^{2+} waves. Such waves are thought to be involved in the synchronization of cells across long distances and typically propagate either via gap junctions or via extracellular messenger release through unpaired gap junctions, or connexin hemichannels. One of the mechanisms of such Ca^{2+} wave propagation involves purinergic signaling [77, 78, 79].

Intercellular signaling mediated by purines appeared early in evolution, thus it is a widespread route for cell-to-cell communication. Purinergic receptors (or purinoceptors) are the most abundant receptors in living organisms and their mechanisms of action play an important part in specialized sensory pathways (Figure 8) [80]. Purinoceptors are divided into ***P1* receptors** that are preferentially activated by adenosine and ***P2* receptors** which are activated by a variety of nucleotides. Additionally, there is recent evidence for the functional expression of adenine receptors, designated as ***P0* receptors** [81, 82]. P1 receptors are G-protein-coupled receptors structured into four receptor subtypes and consist of seven transmembrane domains. P2 receptors are divided into the ligand-gated ion channel P2X receptors that are activated by adenosine triphosphate (ATP) and the G-protein-coupled P2Y receptors (GPCR), which are activated by nucleotides, di- or triphosphates, purines or pyrimidines [83]. P2X receptors are classic cationic ligand-operated channels that upon ATP binding allow the flux of cations such as Na^+, K^+, and Ca^+, playing an essential function in cell signaling and neurotransmitter release. There are seven different P2X receptor subunits ($P2X_1$-$P2X_7$) encoded by seven genes expressed in mammalian cells [84]. The seven subunits have a common topology with two transmembrane (TM) domains, a large extracellular ligand-binding loop, and intracellular N- and C-termini. Each subtype presents a phenotype that is defined by the size, shape and ionic character of

the current and its sensitivity to a range of allosteric modulators, agonists and antagonists [84]. On the other hand, all P2Y receptors share the seven transmembrane-domain topology of G-protein-coupled receptors and are activated by adenine and uridine nucleotides and nucleotide sugars. There are eight subtypes of P2Y receptors that activate intracellular signaling cascades to regulate a variety of cellular processes [80].

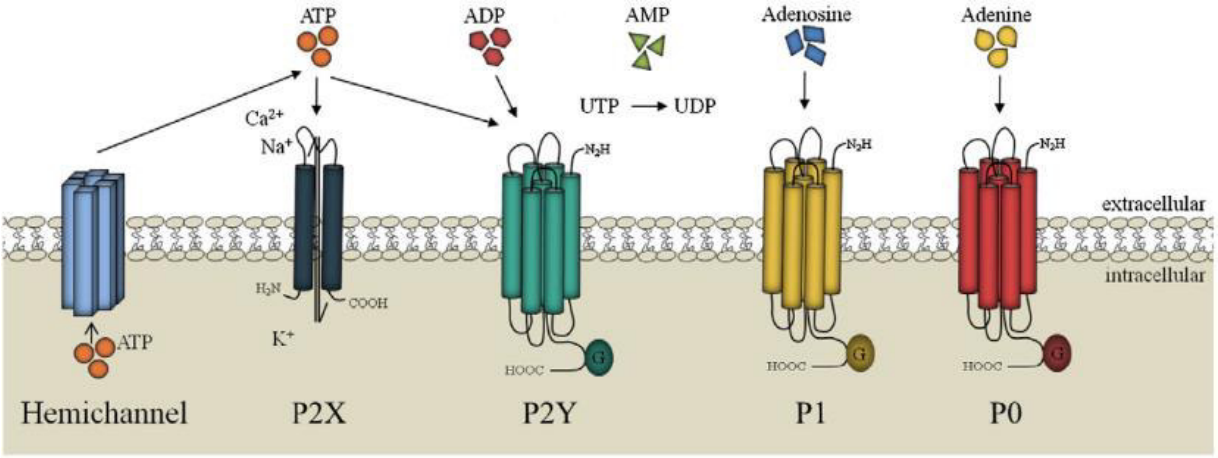

Figure 8. Purinergic receptors and their natural ligands. Gap junctions are unique membrane channels essential in intercellular communication in the developing and mature central nervous system. These channels are composed of connexin proteins that oligomerize into hexamers to form connexons or hemichannels that allow the passive intercellular diffusion of small molecules, such as glutamate, glutathione, glucose, adenosine triphosphate (ATP), cyclic adenosine monophosphate (cAMP), inositol 1,4,5-trisphosphate (IP3), and ions (Ca^{2+}, Na^{+}, K^{+}) P2X receptors activated by ATP while P2Y receptors are stimulated by nucleotides, di- or triphosphates, purines or pyrimidines. P1 receptors are preferentially activated by adenosine. Adenine receptors have been designated as P0 receptors. Modified from *[85]*

Purinergic receptors in the immature cochlea start to be expressed around the second embryonic week and their expression profile and level change until the end of the maturation on the second postnatal week [86, 87, 88]. Köllicker's organ cells exhibit spontaneous Ca^{2+} waves mediated by the spontaneous release of ATP via connexin hemichannels or pannexin channels to act via P2X and P2Y receptors [42, 89, 90] and may allow the establishment of the tonotopic organization of the cochlea and spiral ganglion cell innervation [91]. In the adult OC, several types of both P1 and P2 receptors are expressed in the sensory, supporting and other epithelial cells and are probably involved in their reactions to different stimuli [92] regulating a diversity of primary physiological processes from hearing neurotransmission to cell signaling, OHC motility, gap junctions maintaining and hair cell cation recycling [42, 93, 94, 95].

ATP is released from healthy cells and is considered as an important messenger molecule and modulator in cell-to-cell communication in the central and peripheral nervous system [96]. In the inner ear, ATP is thought to be released spontaneously from Köllicker's organ cells to IHCs [42] and from

Deiters' cells to the OHCs, to act as a co-transmitter with glutamate generating intracellular calcium signals [97]. It has been proposed that an initial local increase of extracellular ATP activates purinergic P2Y receptors, leading to an increase in free intracellular Ca^{2+} concentration $[Ca^{2+}]_i$ [77, 78]. The elevated $[Ca^{2+}]_i$, in turn triggers a release of the intracellular messenger inositol tris-phosphate (IP3) into the cytoplasm which promotes Ca^{2+} release from the endoplasmic reticulum and subsequent Ca^{2+} transfer to mitochondria. ATP is fostered into the extracellular environment (endolymph) through connexin hemichannels. $[Ca^{2+}]_i$ levels are then increased in neighboring cells via at least two distinct mechanisms: (1) IP3 diffusion into neighboring cells via gap junctions triggering an increase in $[Ca^{2+}]_i$ levels; and (2) ATP release into the extracellular environment activating P2 receptors on neighboring cells and leading to a repetition of the cycle (Figure 9) [79]. By acting on purinergic receptors of the hair cells, ATP depolarizes them eliciting glutamate release and activation of the spiral ganglion neurons [87, 95]. Although the spontaneous release of ATP ceases after hearing onset as Köllicker's organ progressively becomes the inner sulcus [26], hair cells and supporting cells in the mature cochlea continue to express P2 receptors [98].

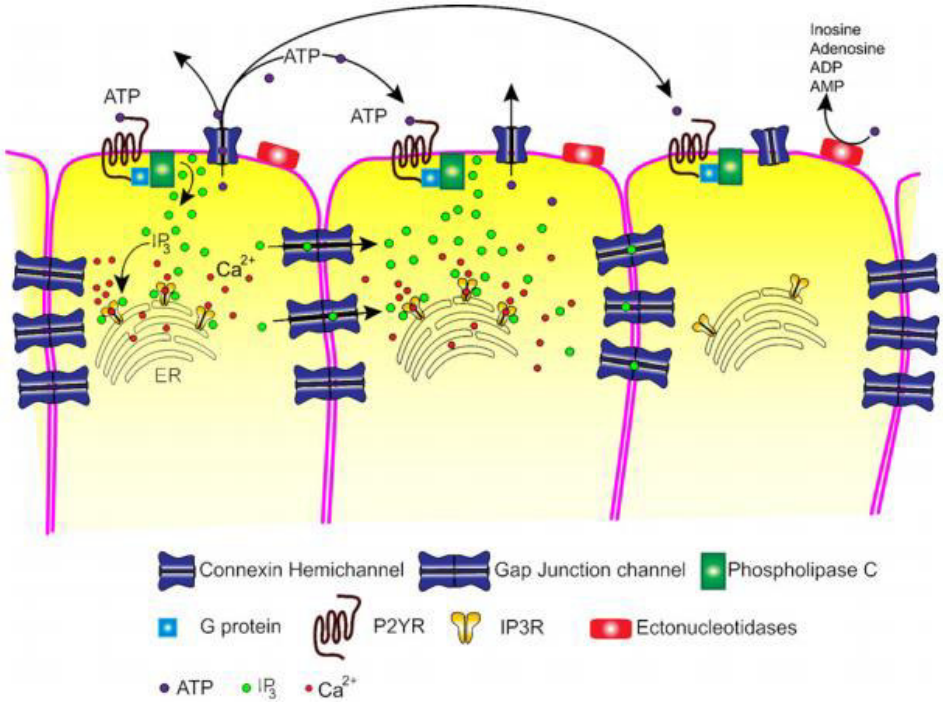

Figure 9. Ca^{2+} signaling in the inner ear. During development, non-sensory cells spontaneously release ATP into the extracellular space through hemichannels, where it activates ionotropic (P2X) and metabotropic receptors (P2YR). IP3R (inositol triphosphate receptor) is a membrane glycoprotein complex; IP3Rs are Ca^{2+} channels in the endoplasmic reticulum (ER) that are activated by IP_3. P2YR are associated with release of Ca^{2+} from intracellular stores (endoplasmic reticulum), whereas P2XR are localized on the stereocilia of the hair cells, as well as in the apical cell surface. ATP degradation by ectonucleotidases terminates signaling. Modified from *[91]*

1.4 iMOP CELLS

Mammalian auditory hair cells are only generated during a short period of embryonic development and are not replaced if lost due to genetic mutations, injury or disease, possibly because of their cell shape, position in a complex tissue or requirement to synapse with neurons. This limited capacity has led to permanent hearing and vestibular impairments for millions of people worldwide [99]. The discovery of neural stem cells and their contribution to continuous neurogenesis in the adult brain provided an experimental paradigm to assay for the presence of stem cells in the inner ear [100].

Cell culture is the technique in which cells are removed from an organism and placed under controlled conditions where they can live and grow. The growth can be characterized by cell division (mitosis) or by other processes, such as differentiation, during which the cells can change into specific types that are capable of functions analogous to tissues or organs in the whole organism. While normal cells usually divide only a limited number of times before losing their ability to proliferate (senescence), a cultured cell line growth can become continuous through a process called transformation, which can occur spontaneously, chemically or virally induced, and can divide indefinitely. Successful cell culture depends on the formulation of appropriate cell culture media and growth conditions [101].

A stem cell is defined by two characteristics: *self-renewal*, the ability to give rise to new stem cells, and *multipotency*, the ability to differentiate into multiple cell types. Mammalian embryonic stem cells and induced pluripotent stem cells can be used to generate functional hair cells and spiral ganglion neurons [20]. Sox2 and the Myc family of transcription factors are crucial for the proper development and self-renewal of inner ear hair cells and neurons. By enhancing gene expression using C-MYC in SOX2-expressing neurosensory precursors, a self-renewing immortalized multipotent otic progenitor (iMOP) line was recently derived [102, 103]. In order to obtain this cell line, murine cochleas were obtained from E11.5-12.5 embryos, during cell cycle exit, and were dissociated into single cells. Dissociated cells were cultured in a defined medium supplemented with bFGF to maintain otic cell identity. To promote long-term self-renewal, exogenous C-MYC was introduced to activate the endogenous *c-Myc* and amplify the transcriptional targets of SOX2, such as the cyclin-dependent kinases. iMOP cells can proliferate as colony-forming cells known as otospheres and have the capacity to differentiate into hair cells, supporting cells and neurons (Figure 10) [102, 103]. Due to the lack of *Oct4*, a crucial factor for pluripotency in embryonic stem cells (ESCs) and in induced pluripotent stem cells (iPSCs), iMOP cells are not pluripotent but are fate restricted and because of the C-MYC and SOX2 presence, iMOP cells

are self-renewing, and capable of differentiating into functional hair cells, supporting cells and neurons. Understanding iMOP cells capacity to differentiate might make this cell lineage be considered as one of the potential tools for cellular replacement therapies in the inner ear.

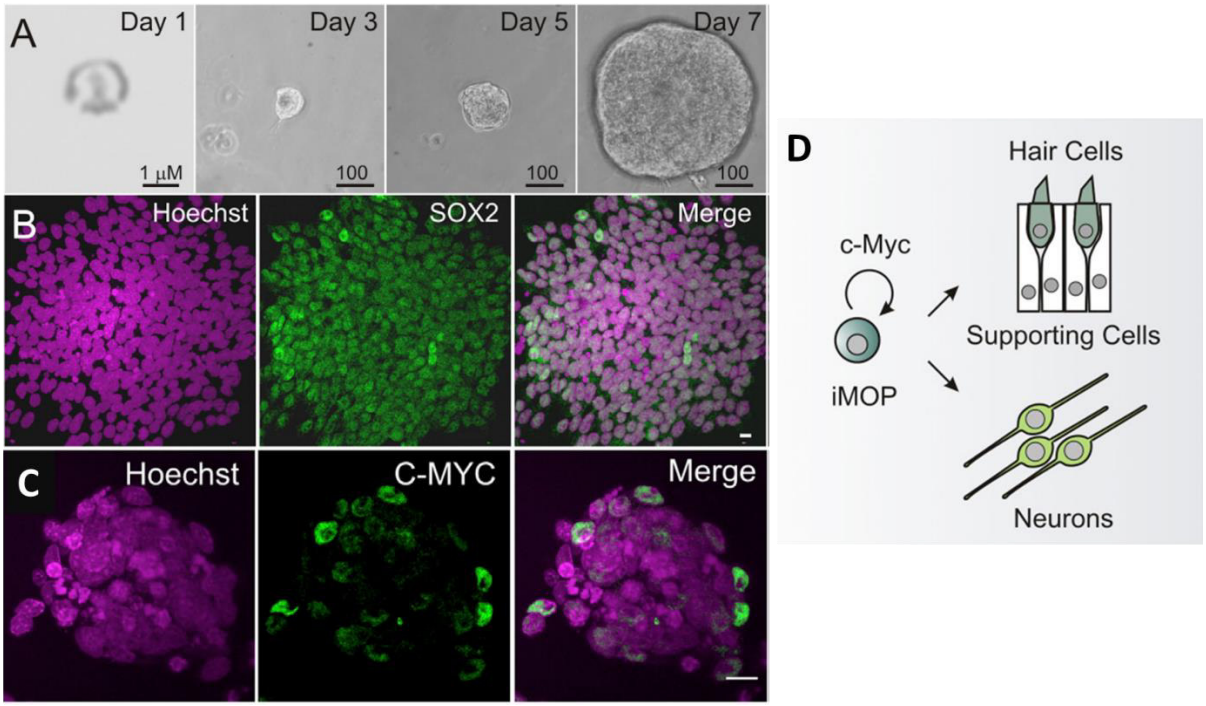

Figure 10. iMOP cells. Hoechst stain labels nuclei and antibody labeling reveals SOX2 and C-MYC. A) Single iMOP cell embedded in Matrigel showing colony formation that progress to multicellular otosphere. B) iMOP colony. Most cells expressed SOX2 in their nuclei. C) In the presence of bFGF, cells expressed C-MYC. D) iMOP cells continually divide but retain the ability to differentiate into functional hair cells and neurons. Modified from *[102]*

1.5 MICROSCOPY & CELL CALCIUM IMAGING

Although the presence of extracellular purinergic signaling in embryonic and stem cells functions has been studied, there is still only sparse information on the role of purinergic receptor expression and regulation during development. Further studies are needed to better characterize the receptor subtypes involved and to identify more precisely the developmental events specifically controlled by purines [104].

As ATP-gated purinergic receptors conduct Ca^{2+}, calcium signaling has been proposed to study purinergic receptor expression. Among the most widely applied methods for studying calcium signaling pathways are the use of fluorescent indicators combined with imaging methods. The applied imaging methods comprise a great variety of fluorescence microscopy, including confocal and two-photon and flow cytometry, while the basis of these methods is the introduction of fluorescent molecules that can form selective and reversible complexes with Ca^{2+} ions (calcium indicators) into the living cells [105]. Particularly, polycarboxylate Ca^{2+} indicators, derived from the selective Ca^{2+} chelator *ethylene glycol-bis(*β*-aminoethyl ether)-N,N,N',N'-tetraacetic acid* (EGTA), such as quin-2, fura-2, indo-1, fluo-3 and fluo-4 have been and are still widely used in *in vitro* calcium signaling studies due to their several advantages over microinjection techniques including simplicity of the loading, fast responses, near-linear responses, and high sensitivities [106, 107]. These fluorescent indicators are polycarboxylate anions which are protected with ester groups, resulting in electrically neutral, lipophilic molecules that pass through the plasma membrane to the cytoplasm. Intracellular esterases cleave the ester, liberating the more polar, polyanionic indicator in the cell that can finally interact with the Ca^{2+} ions [108].

1.5.1 Fluorescence microscopy

For the human eye to perceive details of objects contrast is required. In microscopy, various methods have been developed allowing new applications of optical microscopy in biology. At present, the most popular contrasting technique is fluorescence. Fluorescence is the emission of light that occurs within nanoseconds after absorption, that is typically of shorter wavelength. In fluorescence microscopy the use of fluorochromes or fluorophores is required. Fluorophores are molecules or nanocrystals in which the outermost electron orbitals determine both their efficiency as a fluorescent compound and the wavelengths of absorption and emission. Several different dyes with absorption from the ultraviolet (UV) to the near-infrared (NIR) region are currently available. Fluorescence microscopy excitation

requires a specific light source, subsequent separation of the relatively weak emission from the strong exciting light and, finally, detection of fluorescence. An efficient separation of the exciting light from the fluorescence light, which eventually reaches the observer's eye or the electronic detector, is necessary for obtaining high image contrast [109].

1.5.2 Fluo-4

Fluo-4 (Figure 11) is one of many Ca^{2+} indicators known as single wavelength dyes, that is their measurements are restricted to one excitation and one emission wavelength. The advantage of this approach is that successive images may be collected with a minimum delay between measurements. Fluo-4 was synthesized similarly to Fluo-3 [110] but two fluorines were substituted for the two chlorine substituents in the fluorophore. This modification yields greater absorbance around 488 nm [111] thus making it excitable by the argon-ion laser generating more intense fluorescence and reducing photobleaching of the dye and lowering the cellular phototoxicity due to the reduction of the excitation light intensity.

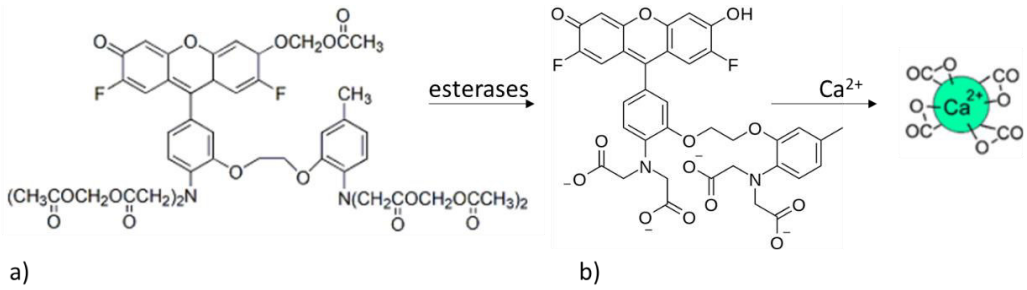

Figure 11. Skeletal formulas of Fluo-4. a) Chemical structure of Fluo-4 b) Tetradeprotonated Fluo-4 after esterases have cleaved AM groups. Fluo-4 exhibits large fluorescence intensity increases on binding Ca^{2+}. Complete hydrolysis of the AM esters is very important to avoid artefacts. *Modified from [112]*

Fluo-4 is essentially nonfluorescent without Ca^{2+} present and responds to Ca^{2+} binding with an increase of fluorescence intensity but no spectral shift. Fluo-4 and similar fluorophores are restricted to measurements of relative [Ca^{2+}] changes within and among cells and for measuring high transient Ca^{2+} concentration during Ca^{2+} spikes as a quantitative measurement is much more difficult. In general, calcium indicators are unable to cross lipid membranes due to their nature but the protection of acetoxymethyl (AM) esters in Fluo-4 makes the dye neutral and it can be passively loaded into cells via incubation. Fluo-4 dissociation constant for Ca^{2+} – K_d (Ca^{2+}) is 345 nM. Once inside the cell, esterases will cleave AM groups (Figure 11) [112].

1.5.3 Laser scanning confocal microscopy

Confocal microscopy is an optical imaging technique for visualization and quantification of three-dimensional structures as it can optically section the specimen. It is a type of fluorescence microscopy that requires certain optical components to generate high-resolution images of samples labeled with fluorescent probes. Typically, in common widefield fluorescence microscopy, the sample is completely illuminated by the excitation light, thus all the sample is fluorescing at the same time contributing to a background haze in the resulting image [113].

Unlike widefield fluorescence microscopy, the confocal microscopy optical path is designed so that a circular aperture (pinhole) is placed in front of the image detector (photomultiplier tube or camera) at a point where the image is focused in conjugated planes with the focal plane of the image (Figure 12). If this aperture is correctly placed in the same focal position as the collected image and the size of the aperture is adjusted to match the numerical aperture of the objective lens that is collecting the image, it is possible to screen out light from outside the true focal plane of the objective lens. The term confocal derives from the coincidence of these two conjugate focal planes (objective lens focus point and the focus point where the aperture is placed). By having a confocal pinhole, the microscope is efficient at rejecting out of focus fluorescent light producing a neat image with the maximal resolution possible for the objective lens being used. The practical effect of this is that the image comes from a thin section of the sample [114].

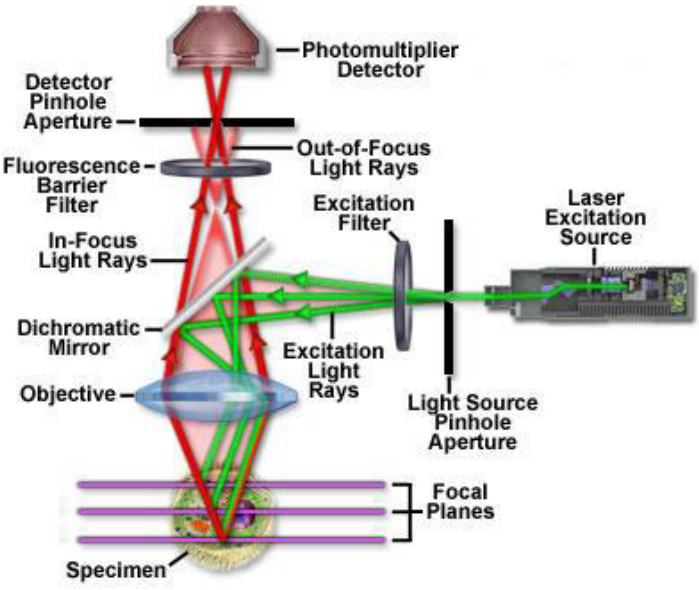

Figure 12 Laser scanning confocal microscope optical configuration. Coherent light emitted by the laser system passes through a pinhole aperture that is in a confocal plane with a scanning point on the specimen and a second pinhole aperture positioned in front of the detector (a photomultiplier tube). As the laser is reflected by a dichromatic mirror and scanned

across the specimen in a defined focal plane, secondary fluorescence emitted from points on the specimen (in the same focal plane) pass back through the dichromatic mirror and are focused as a confocal point at the detector pinhole aperture. From *[115]*

Besides the placement of the pinhole at the precise point in the light path, the light source must be of high intensity and provide for specific wavelengths of illumination. A combination of lasers is the most common way to provide a distribution of excitation illumination across the visible spectrum, thus referred to as laser scanning confocal microscopes (LSCM). LSCM image the sample using two galvanometer mirrors that focus and direct the laser beam to scan a desired focal plane. Any out-out-of-focus emission signal that is not aligned to the objective focal point is eliminated by the pinhole. Once the laser beam has scanned in x-axis, it is returned to its initial position where a second galvanometer mirror directs it in the y-axis. This process is repeated line by line so that the specimen is scanned pixel by pixel in the *xy* dimensions [116]. The emitted light from the activated fluorophore is then collected by the objective lens, it passes through an emission filter to narrow the signal before being focused through the aperture onto a photomultiplier tube, which acts as a light detector (Figure 12). By scanning many thin sections through the sample, a very clean three-dimensional image of the sample can be built up [114].

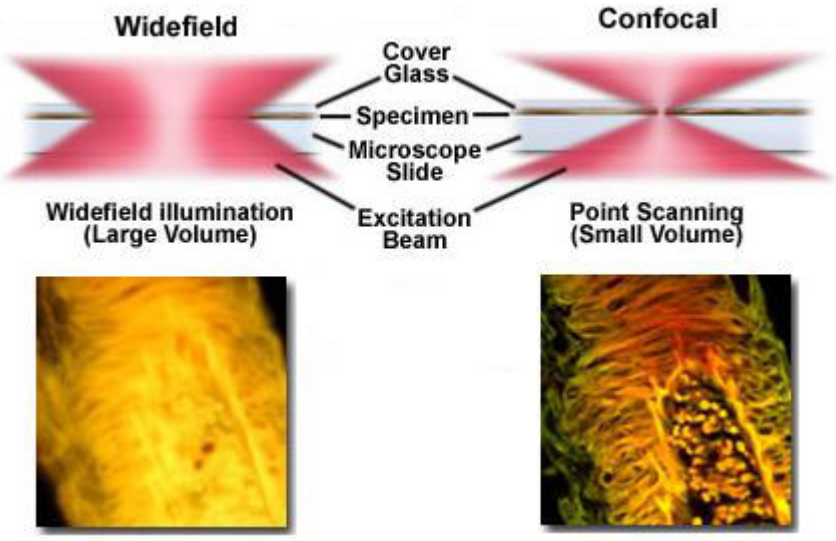

Figure 13. Confocal and widefield fluorescence microscopy. Widefield microscope objectives focus a wide cone of illumination over a large volume of the specimen, which is uniformly and simultaneously illuminated. The laser illumination source in confocal microscopy is first expanded to fill the objective rear aperture and then focused by the lens system to a very small spot at the focal plane. A thick section of fluorescently stained human medulla in widefield fluorescence exhibits a large amount of glare from fluorescent structures above and below the focal plane. When imaged with a laser scanning confocal microscope, the medulla thick section reveals a significant degree of structural detail. Modified from *[115]*

2. STATEMENT

Purinergic signaling is present from the earliest developmental stages of acquisition of hearing, which involves differentiation, proper organization, and functional maturation of the cochlear cells. To date, there are only few studies implicating extracellular purines and pyrimidines in embryonic and stem cell functions. Specifically, on otic progenitors, no studies of the presence of purinoceptors have been found published. Due to the importance of these receptors during cell development, it is hypothesized that the iMOP cell line must have P2X receptors, therefore ATP should trigger a response.

3. AIMS

The main aim of the present work is to study iMOP cells' response to purinergic receptors stimulation to determine the existence or absence of functional purinergic receptors on these cells.

Objectives:

1. To identify the presence of P2X purinergic receptors in iMOP otospheres by stimulating them with ATP and using a calcium indicator to observe the response
2. To observe iMOP behavior in the presence of the compounds used during calcium signaling experiments by exposing the cells separately to each reagent listed on the protocol to make sure that there are no adverse effects
3. To classify the measurements of the responses to ATP stimulation in a qualitative way based on the fluorescence intensity and in a quantitative way by means of a spectral analysis to find a pattern to identify a response due to the presence of ATP

4. MATERIALS AND METHODS

4.1 CELL CULTURE

4.1.1 Maintaining, freezing and thawing iMOP cells

iMOP cells were grown in iMOP culture media containing Dulbecco's Modified Eagle Medium: Nutrient Mixture F-12 (DMEM/F-12), 1X B-27 supplement, 25 µg/mL carbenicillin and 20 ng/mL basic Fibroblast Growth Factor (bFGF) in 60 mm sterile culture dishes at 37°C with 5% CO_2. The passage was made every 7 days by transferring the whole culture to a conical tube. Cells were harvested by gravity sedimentation placing the conical tube containing the culture at 37°C for 5 min. After that time, the spent medium was removed without disturbing the cell pellet collected at the bottom of the tube. To facilitate dissociation into single cells, 0.5 mL of pre-warmed 1 mM ethylenediaminetetraacetic acid - Hanks' balanced salt solution (EDTA-HBSS) solution were added to the cell pellet and gently pipetted up and down 2-3 times with the 1 mL pipette. The tube was then placed at 37°C and incubated there for 5 min. Next, 2 mL of iMOP culture media were added to neutralize and dilute the EDTA. Cells were collected by centrifugation at 200 x G for 5 min at room temperature (RT). The diluted EDTA was removed and 5 mL of 1X Phosphate Buffered Saline (PBS) were added to wash the cells. Then, iMOP cells were centrifuged again at 200 x G for 5 min at RT and the supernatant was removed. Cells were resuspended in 1 mL of iMOP culture medium by gently pipetting up and down 2-3 times. Cells were counted by placing 11 µL in a Neubauer counting chamber under an Axio Observer.A1 inverted microscope (Zeiss, Germany) with the help of a tally counter. 2.5 x 10^5 cells were plated in a 60 mm dish in iMOP culture media. Two mL of fresh medium was added to iMOP cells every other day without removing any medium.

For cryopreservation, cells were collected by gravity sedimentation at 37°C for 5 min, the spent medium was removed, and the cell pellet was resuspended at a density of ~5 X 10^5 to 3 X 10^6 cells/mL in 4°C synthetic freezing media (Synth-a-Freeze Cryopreservation Medium, Thermo Fischer Scientific A1254201). The cell suspension was transferred to cryogenic vials and placed in an alcohol-free freezing container at -80°C. For long-term storage, vials were transferred to a vapor phase of a liquid nitrogen storage tank. To thaw out cells for culture, the cryogenic vial containing frozen cells was equilibrated at -80°C overnight. The frozen vial was quickly thawed by swirling the bottom of the vial in a 37°C water

bath. One mL of pre-warmed iMOP culture medium was added to the thawed cells once the last ice crystal disappeared. Then, the cells were transferred into a conical tube and an additional 4 mL of iMOP culture medium were added. The tube was centrifuged for 5 min at 200 x G and the diluted freezing medium was removed. Finally, cells were resuspended in 2 mL of iMOP culture medium and plated in a 60 mm culture dish.

4.1.2 Differentiating iMOP cells into Sensory Epithelium

In order to differentiate iMOP cells into sensory epithelium cells, the iMOP sensory epithelium differentiation medium was prepared using DMEM/F12, 1X B27 supplement and 25 µg/mL carbenicillin. Cells were harvested, dissociated, resuspended and counted as in the maintenance protocol. 2.5 x 10^5 cells were plated in a 60 mm dish on *Day -3* using iMOP culture medium. On *Day 0*, cultures were transferred into a conical tube. Otospheres were collected by gravity sedimentation for 5 min, spent medium was removed and 2 mL of sensory epithelium differentiation medium were added. Cells were then transferred to a 60 mm dish. Two mL of fresh sensory epithelium differentiation medium were added to the culture every other day; the cells were collected on *Day 10* for fixation.

4.1.3 Differentiating iMOP cells into Neurons

As iMOP cells become adherent when differentiating into neurons, coated coverslips were prepared so cells could attach to them. Glass coverslips were cleaned with 70% EtOH for 10 min at RT and then rinsed 3 times with 1X PBS to wash out the remaining ethanol. Coverslips were once rinsed with H_2O to wash out remaining 1X PBS and let them dry before exposing them to UV light in the culture hood for 15 min. 250 µL of 10 µg/mL poly-D-lysine in 1X PBS were placed on coverslips and left at 37°C for 1 h; the coverslips were then washed 3 times in 1X PBS. Next, 250 µL of 10 µg/mL laminin were placed on coverslips and left at 37°C overnight. The following day, laminin was removed, and coverslips were rinsed 3 times with 1X PBS.

To initiate neuronal differentiation, the neuronal differentiation medium was prepared with Neurobasal medium, 1X B27 supplement and 2 mM Glutamax. Cells were harvested, dissociated and counted as in the maintenance protocol. 1 x 10^6 cells were plated in a 60 mm dish at *Day -3* and on *Day 0*, iMOP cells were harvested, dissociated and counted again. 1 – 1.5 x 10^5 iMOP cells were seeded into each well of a 12-well dish, containing 1 mL of pre-warmed neuronal differentiation medium and

coated coverslips. The medium was aspirated and fresh medium was added to cultures every other day. Coverslips with cells were fixed on *Day 7*.

4.1.4 Fixing, staining and mounting iMOP cells

After 10 days, for sensory epithelium cultures, otospheres were collected by transferring to a conical tube and allowing them to sediment as stated before, then spent media was removed and otospheres were fixed by incubating in freshly prepared 4% formaldehyde in 1X PBS for 30 min at RT. Similarly, after 7 days, for neuronal cultures, coverslips were fixed by incubating in freshly prepared 4% formaldehyde in 1X PBS for 30 min at RT. Formaldehyde solution was removed and to permeabilize the membrane, otospheres were washed with 1X PBS containing 0.1% Triton X-100 3 times for 10 min each time. In order to wash otospheres, cells were centrifuged at 200 x G for 1 min between each wash.

For immunostaining, cells were incubated in blocking solution containing 1X PBS, 10% (vol/vol) goat serum and 0.1% Triton X-100 for 1 h at RT. The supernatant was removed and then, primary antibodies properly diluted in blocking solution (see Graph 2.1) were incubated with cells overnight at 4˚C. After incubation, cells were washed in 1X PBS containing 0.1% Triton X-100 3 times for 10 min each time. Then, the appropriate secondary antibody fluorophore (Graph 2.1) was diluted in blocking solution and incubated for 2 h at RT. Additional stains: Hoechst 33258 (Molecular Probes No. H3569) 1:500 for 10 minutes; Alexa Fluor™ 488 phalloidin (Thermo Fisher Scientific, No. A12379) 1:200 or Alexa Fluor™ 647 phalloidin (Thermo Fisher Scientific, No. A22287) 1:200 for 20 min were added to the incubating solution or directly diluted in PBS when antibodies were not used, before secondary antibody incubation time ended. Next, cells were centrifuged and washed in 1X PBS containing 0.1% Triton X-100 3 times for 10 min each time and rinsed once in 1X PBS to get rid of excess detergent before mounting.

Graph 2.1 Dilutions of primary and secondary antibodies used for immunostaining

Primary antibodies		Secondary antibodies	
Anti-Neurofilament 200 (rabbit host) Sigma-Aldrich No. N4142	1/200 dilution	**Alexa Fluor™ 488** goat α-rabbit Invitrogen No. A11070	1/200 dilution
Anti-Tubulin polyclonal (sheep host) Cytoskeleton No. ATN02	1/500 dilution	**Alexa Fluor™ 488** monkey α-sheep Themo Fisher Scientific No. A-11015	1/200 dilution

Finally, to mount the cells for observation, one drop of Prolong Diamond Anti-Fade was placed on a slide and the coverslip was placed upside down on top of the mounting medium. In the case of otospheres, PBS was removed leaving only ~50 µL of solution. Cells were gently resuspended in the remaining PBS and placed onto a slide. The solution was left for ~1 min so that the cells could somehow adhere to the slide. Then a drop of Prolong Diamond Anti-Fade was placed onto the cells and left to equilibrate for ~1 min before putting a clean coverslip on top. Both types of samples were left to dry at 4°C.

For image acquisition, samples were observed in an LSM-710-NLO confocal microscope (Zeiss, Germany) equipped with LCI Plan-Neofluar 25x/0.8 Imm Korr DIC M27 and alpha Plan-Apochromat 63x/1.46 Oil Korr M27 immersion objectives. The light sources used for imaging were: HeNe 633 laser for Alexa Fluor™ 647, Ar laser (488 nm laser line) for Alexa Fluor™ 488; and 405 diode laser for Hoechst. Images were processed using the FIJI open-source platform for biological-image analysis.

4.2 CALCIUM IMAGING

As a summary of the procedure to perform the calcium signaling experiments, a flowchart was created and is shown in Figure 14. The oval figures show the beginning and end of the procedure, starting with the cell culture and obtaining graphs from the fluorescent and spectral analysis as the main output. The arrows indicate the direction of the flow and the black dots indicate junction. The rhombuses express the need to make a decision; in the first rhombus it is decided if a file is discarded or not depending on the position of the otospheres. If an otosphere is out of focus or becomes out of focus throughout the video, the file is discarded. The turbulence is another important aspect, if the otosphere can’t be tracked, the file is discarded. In the second rhombus the decision is made depending on the number of images with turbulence, if more than 10 frames show turbulence, the file is discarded. Finally, the dotted rectangles indicate the discarded data (flowchart output).

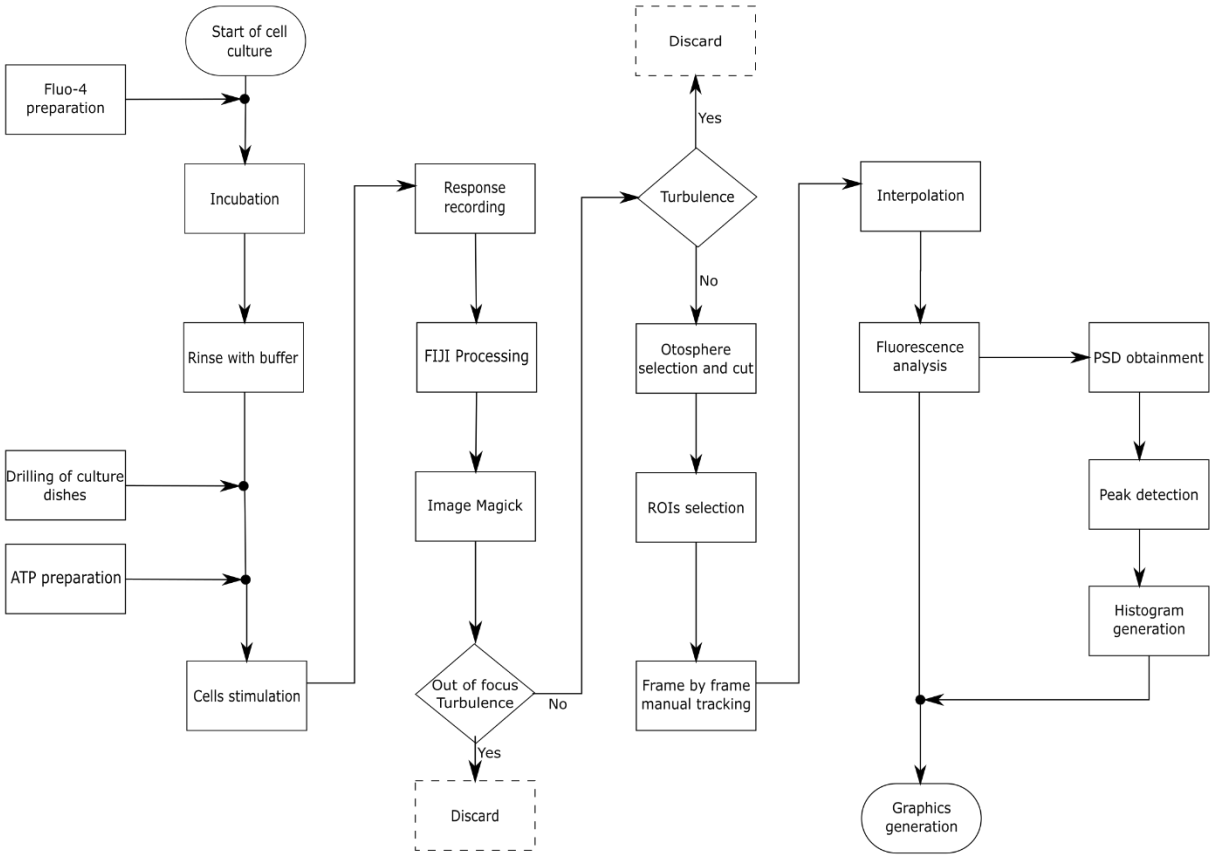

Figure 14. Flowchart summarizing the section 4.2 of the Materials and Methods chapter. Black dots indicate junction, rhombuses indicate the need to make a decision, the ovals show the beginning and end of the flow chart, the arrows indicate the direction of the flow and the dotted figures show discarded data.

To observe the cells in the confocal microscope and to limit the movement of the floating otospheres, glass bottom wells (Figure 15) were prepared in culture dishes as follows. Using a 2.4 mm engraving cutter on a Dremel© 3000, four holes were drilled in 35 mm culture dishes. Glass coverslips were sticked at the bottom of the drilled dishes using the silicone elastomer Sylgard™184 and left to dry overnight at 75°C. Then, the dishes were once washed in distilled water for 10 min and washed with 70% EtOH three times for 30 min each time. Next, the dishes were sterilized under UV light for 30 min before coating the wells with 12 µL of 10 µg/µL poly-D-lysine for 1 hr at 37°C. Poly-D-Lysine was then removed and the newly prepared wells were filled with HBSS free of Ca^{2+} and Mg^{2+} until use.

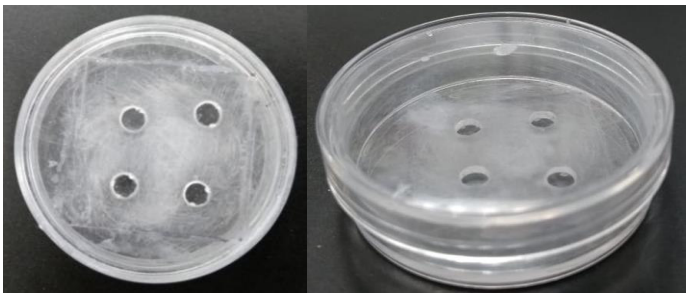

Figure 15. 35 mm drilled culture dishes ready to use for calcium imaging acquisition.

The Fluo-4 AM stock solution was prepared by dissolving 50 µg of the Ca^{2+} indicator Fluo-4 AM with 50 µL of dimethyl sulfoxide (DMSO). This stock solution was stored at –20°C and thawed at 4°C before use. The loading solution was freshly prepared by adding 2 µL of Fluo-4 AM stock solution to 2 µL of 20% Pluronic F-127 and dissolving in 1 mL of pre-warmed HBSS free of Ca^{2+} and Mg^{2+}.

ATP solutions were prepared by dissolving ATP at different concentrations (50 mM, 5 mM, 500 µM, 50 µM, 5 µM, 500 nM, 50 nM and 5 nM) in HBSS free of Ca^{2+} and Mg^{2+}. $CaCl_2$ was also prepared at different concentrations (3.5, 2, 1.5, 1, 0.5, 0.2 and 0.05 mM) in HBSS free of Ca^{2+} and Mg^{2+}.

For experiments, iMOP cultures were placed lopsidedly for 5 min so that the otospheres would sediment on one side of the dish and the medium could be removed without disturbing the cells. Then, the otospheres were washed with HBSS free of Ca^{2+} and Mg^{2+} maintaining the dish inclined for 2 min. HBSS was removed and the loading solution was added without moving the dish position. The cells were incubated for 30 min at 37 °C, then washed again in HBSS and kept in HBSS free of Ca^{2+} and Mg^{2+}. Cells were then transferred to the glass bottom wells by adding 10 µL of loaded cells per well.

Cells were observed with the LSM-710-NLO confocal microscope (Zeiss, Germany) using the 25x immersion objective, the Ar laser at 488 nm and a wide-open pinhole at 9 airy units (AU) or 2.4 µm. Otospheres were focused on an optical slice where a majority of loaded cells (fluorescent) could be seen. The “Time Sequence” option was programmed to run for 250 cycles in 2 min, resulting in 250 images. In some cases, it was run for 120 cycles in 1 min. Cells were stimulated by manually applying 4 µL of ATP ~10 sec after the start of the sequence.

Both pseudo brightfield and fluorescence channels were saved as raw files of 128 500 KB each one with the CZI format in the Zen Microscope software (Zeiss, Germany). CZI is a proprietary binary format which saves multidimensional images combining imaging data with relevant meta information. The files

were then processed using the FIJI open-source platform for biological-image analysis to split both channels and to generate AVI files which could be analyzed using customized routines developed with Python 3.7v and Ruby 2.7v programming languages. These routines were generated in collaboration with MSc. Ricardo Nieto Fuentes (doctoral student at CIMAT, A.C.) by using Image Magick free and open-source software suite for the conversion of AVI files to PNG files; the Ruby 2.7v programming language to benefit from its API of the TK library for the graphical user interface and the Matplotlib and SciPy libraries from Phyton 3.7v for graphics generation and signal analysis. The pseudo brightfield channel images were used to track the iMOP cells throughout the video but the fluorescence channel information was used to proceed with the fluorescence analysis.

Videos showed that when ATP solution was added to the wells containing floating iMOP spheres, turbulence was generated and consequently spheres moved. Turbulence produced image noise and as Figure 16 shows, otospheres could not be followed due to dimming frames. In order to avoid noise when graphing fluorescence variation, blurry images had to be removed and missing data were filled by doing an interpolation from the data of the image prior to ATP stimulation and the first clear image: $\frac{\Delta f}{\Delta t}(t - t_0) + f_0$, where f is the fluorescence and t the time. In the case of Figure 16, only Figure 16 B and C were discarded, Figure 16 D was considered a clear image. If more than 8 images had to be dismissed from a recording, the complete video was not considered for the analysis.

The analysis program is designed to plot fluorescence intensity variations ($\frac{\Delta F}{F_0}$) from specific regions of interest (ROIs) over time. ROIs were first chosen as of the regions where fluorescence intensity variations over time were obvious to the naked eye. Once these regions were picked, the rest of the ROIs were distributed along the sphere. As shown in Figure 17 A, ten circle-shaped ROIs were manually traced over a single iMOP sphere on the first image of each video. Due to the movement of the floating otospheres over time, mainly after ATP stimulation, videos were analyzed frame by frame and ROIs were manually tracked. To facilitate the ROIs selection and tracking, the user interface shows the merged images (pseudo brightfield + fluorescence channels) but the analysis was performed only on the fluorescence channel images.

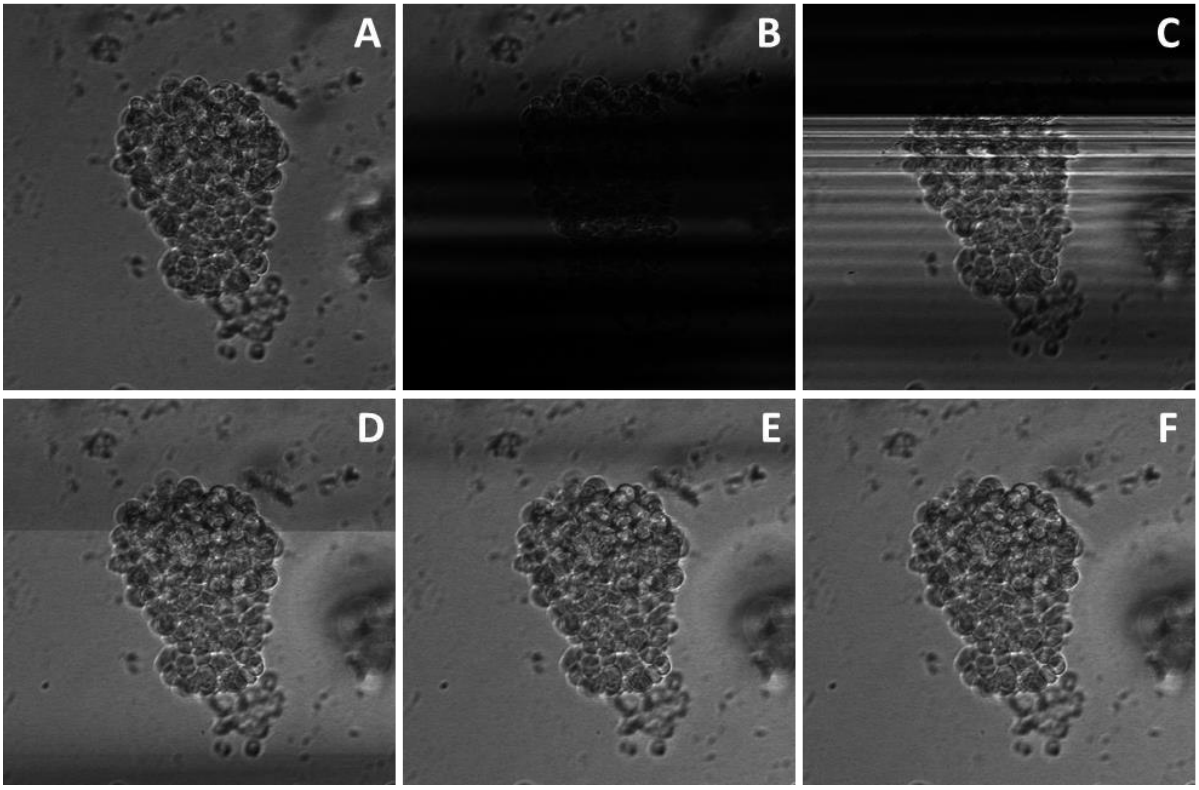

Figure 16. Video frames extracted from a time sequence of an experiment shows that turbulence is generated by ATP solution was added to wells containing iMOP cells. No image noise is detected prior to ATP stimulation (A). When the ATP drop reaches the wells, turbulence is generated producing dimming images (B & C). Once the fluids got back to stable, clear images are seen again (D-F).

The fluorescence change was defined as a delta function of $\frac{\Delta F}{F_0} = \frac{F_{(t)} - F_0}{F_0}$, where F_0 is the average fluorescence intensity of the ROI in the first image of recording and $F_{(t)}$ is the average fluorescence intensity at a given time. Therefore, ΔF indicates the difference between initial fluorescence intensity at the resting state and after stimulation. An example of fluorescence relative change in time is shown in Figure 17 B, where the color of each curve corresponds to the color of the ROI established in Figure 17 A.

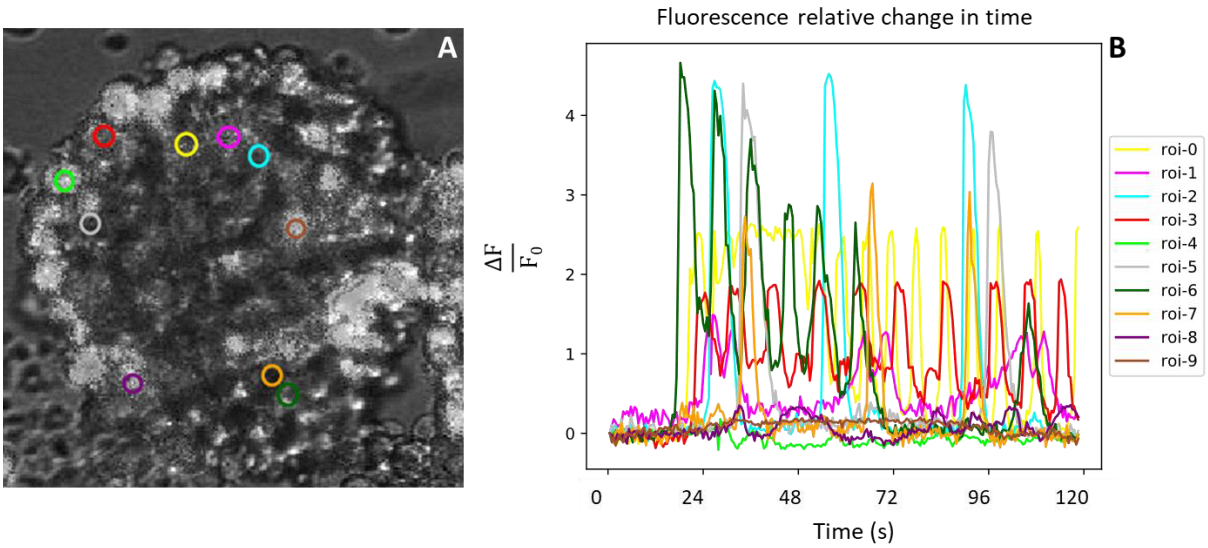

Figure 17. Representative fluorescence intensity variations analysis. ROIs selection (A) was manually done followed by frame by frame tracking. 10 regions were chosen per otosphere. The color of each ROI matches the color of a curve in the fluorescence relative change in time graph (B). All recordings were 120 s long at a frequency of two images per second.

Figure 18 explains how the program works and how the graphs are generated. A ROI is selected within the otosphere (Figure 18 A) and tracked over time (Figure 18 C-E). Fluo-4 results in a fluorescence intensity increase in response to Ca^{2+} binding. If cells stimulation with ATP produces a fluorescence intensity increase in the selected ROI, it will be represented as a peak (Figure 18 B) in the time-course graph. Fluorescence variations can also be observed in the videos as changing intensity sparks (Figure 18 C & E). In Figure 18 the fluorescent channel was pseudo-colored in an RGB (red green blue) color model. Intensities are measured in arbitrary fluorescence units. The analysis program is available online at https://gitlab.com/imop-fluorescence-analysis

In order to establish a baseline, iMOP cells were incubated in the Fluo-4 solution as aforementioned and two-minute videos were recorded. No stimulation was applied for this purpose and ROIs analysis was performed in the same way.

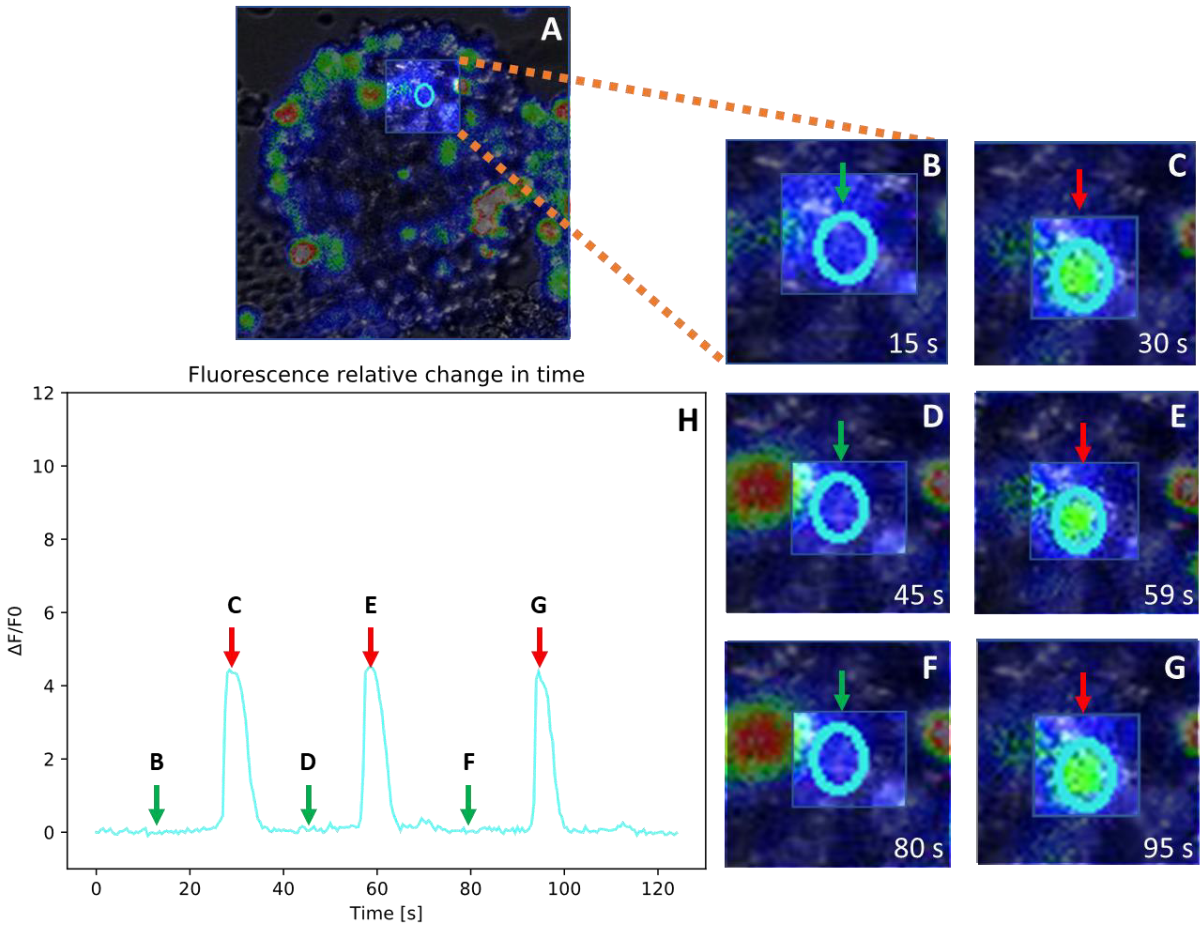

Figure 18. Analysis program graphical example. After recording 2 min videos, regions of interest (ROIs) were manually set (A), tracked frame by frame(B-G) and $\Delta F/F_0$ over time was graphed (H). For a better visualization, a close up of a single ROI (A-B) was made, the following frames show the same close up at different time points. Peaks on the graph can be detected on videos as a fluorescent intensity variation and are indicated with red arrows on the graph (C, E, G). Valleys indicating an absence of fluorescence intensity variation, are shown with green arrows (B, D, F).

To determine Ca^{2+} oscillations frequencies, spectral analysis was performed according to a previously reported method [117]. Spectral analysis is commonly based on the Fourier transform where data collected in the time domain is transformed to information into the frequency domain. A spectral analysis program using Phyton was created based on a code written for MATLAB which computes the fast Fourier transform (FFT) on the previously acquired Ca^{2+}-signaling data [117]. To do this, ROIs recorded data were imported into the program and the trend component of the experiment was determined and subtracted, also, the time difference between each sample was indicated (dt= 0.5s). Then, the FFT was calculated and the power spectral density (PSD) was obtained. The discrete-time version of the Fourier transform, which operates on time domain signals that are sampled at specific time-intervals, is shown as

$$G(f_k) = \sum_{n=1}^{N} g(t_n) e^{-i2\pi kn/N} \qquad k = 1 - \frac{N}{2}, \ldots, \frac{N}{2}$$

Equation 1

where $g(t_n)$ represents the original signal in the time domain, $G(f_k)$ represents the Fourier transform in the frequency domain, and $e^{-i2\pi kn/N}$ is a function containing both real and imaginary part. To identify and quantify oscillatory patterns within the Ca^{2+} recordings, a power spectrum was defined. PSD is the measure of a signal's power intensity in the frequency domain, it is computed from the FFT spectrum of the signal and is defined as

$$P(f_k) = \frac{1}{N} |G(f_k)|^2$$

Equation 2

where *N* is the number of samples. PSD data were mapped onto a frequency array that shows how much signal is present per unit of bandwidth. Next, relative power was calculated to determine the most dominant frequencies (it tells how much power one peak holds in relation to the total power of the spectrum). Line graphs indicating the most relevant peaks were generated. A histogram that contains the average values of PSD and a histogram containing the number of occurrences of a frequency in the data were also generated and saved as SVG files.

5. RESULTS

5.1 CONFOCAL MICROSCOPY

As iMOP cells were recently established [103] and are new to our laboratory, one of the first challenges was to start and maintain an iMOP cell culture before initiating with further experiments. In order to get familiar with the morphology of this cell line, growth was tracked (Figure 19) and compared to the results published by Azadeh et al [103]. Some adjustments were made, mainly on the number of plated cells on passage day as iMOP growth rate was faster in our laboratory.

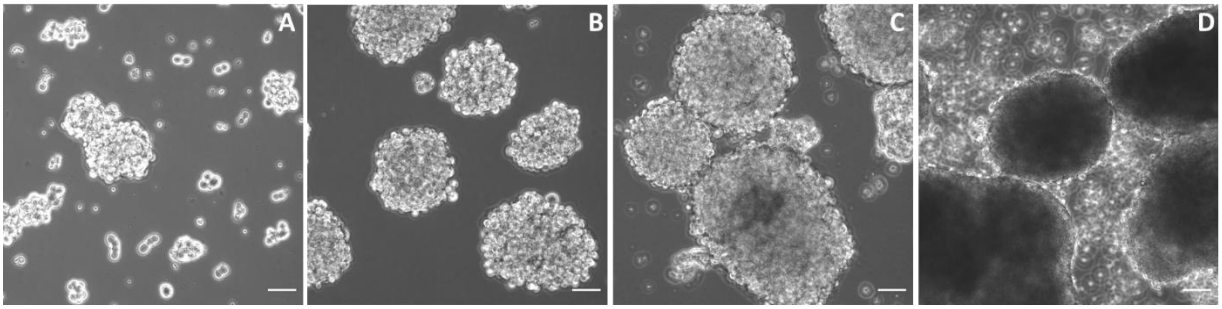

Figure 19. Phase contrast images of otospheres on day 1 (A), 3 (B), 5 (C) and 7 (D). Length of scale bar is 50 µm.

Once iMOP cells were proliferative, their capacity to differentiate into supporting cells and spiral ganglion neurons (SGNs) was monitored. bFGF was withdrawn from the culture and cells were fluorescently labeled to highlight morphological features of the differentiated cells.

As shown in Figure 20 B and E, cell nuclei show slight differences in specific patterns after differentiation into iMOP-derived sensory epithelia most likely due to chromatin changes. As these cells have been cultured for a long time, dying cells may also be present in the larger spheres showing fragmented nuclei. Representative images of iMOP-derived neurons display morphological changes like long neurites extending from cell bodies by day 7 (Figure 20 G-I). Further tests using cell cycle exit and expression of early-stage markers for sensory epithelial and neurons (such as Cdkn1b ($p27^{KIP}$) and Cdh1) are suggested to be used to evaluate the differentiation potential of the cells.

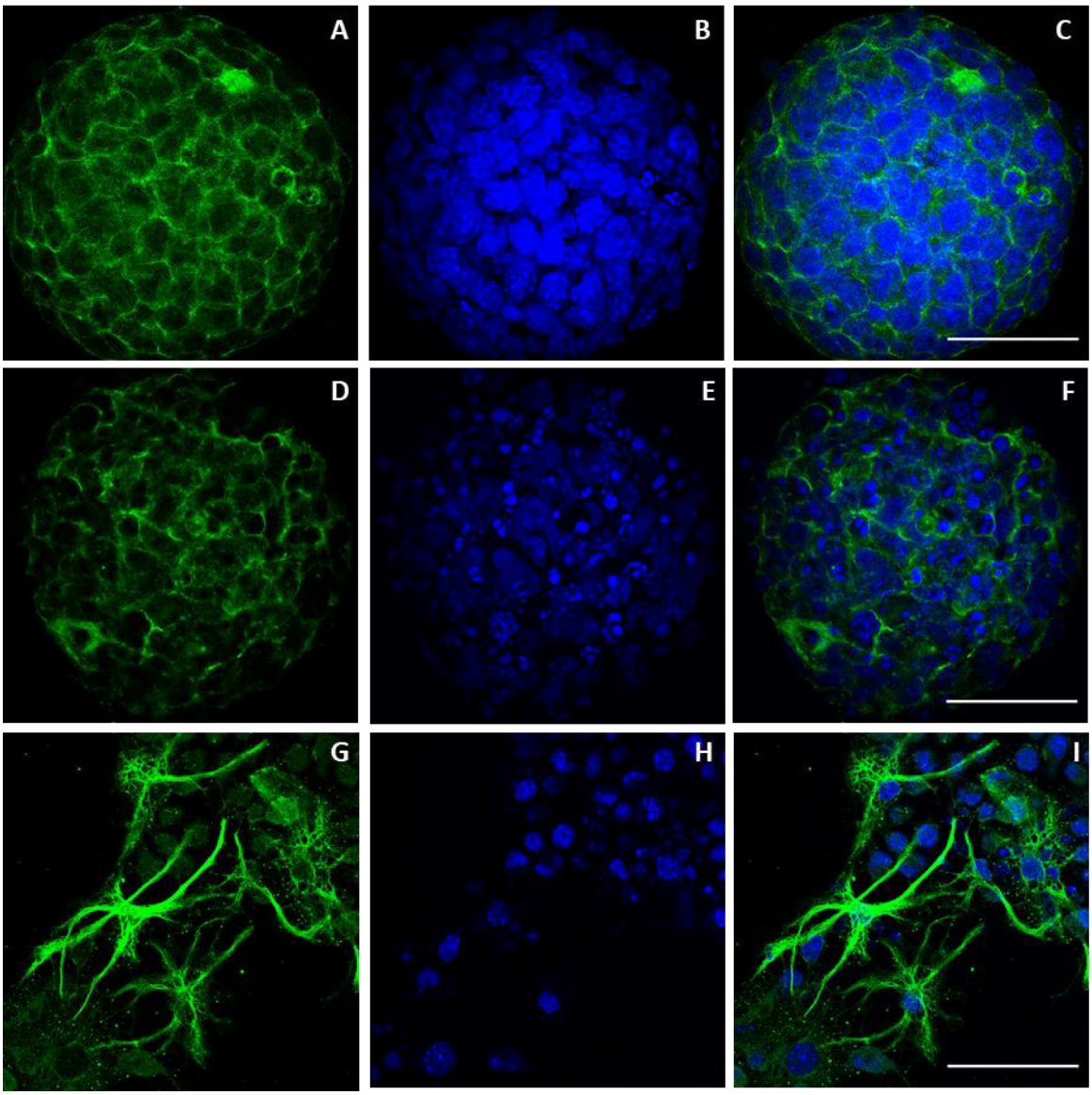

Figure 20. iMOP cells cultures confocal micrographs. iMOP-derived otosphere cultured in the presence of bFGF for 7 days (A-C) and in sensory epithelia culture media for 10 days (D-F). Filamentous actin was labeled with (A and D) phalloidin (actin filaments). Nuclei of cells were labeled with (B & E) Hoechst. (C and F) The merged image of iMOP cells. iMOP cells after 10 days of neuronal differentiation (G-I). Neurofilaments were labeled with Alexa Fluor™488 (G) and nuclei were labeled with Hoechst (H). Merged image of iMOP-derived neurons. Scale bar is 50 µm.

5.2 CALCIUM IMAGING

As there is limited data on calcium signaling in pluripotent stem cells and in order to get to know the sensitivity of iMOP cells, otospheres were subjected to some tests before starting with calcium imaging protocols.

During cochlear development, cells within Kölliker's organ have been reported to show a decrease in light transmittance ('darkening') due to crenation correlated with intracellular Ca^{2+} waves [89, 118]. In the interest of studying if optical changes occur on iMOP cells after a rise in $[Ca^{2+}]_i$, $CaCl_2$ solutions were prepared at different concentrations during different time intervals and were tested replacing the growth medium. Cells were immediately checked after replacement and 10 min, 20 min, 30 min, and 60 min after stimulation with $CaCl_2$. As no darkening or any other morphological change was seen at any calcium concentration, the longest time interval is shown in Figure 21. Crenation may be caused by the efflux of Cl^- followed by water after Ca^{2+} activated Cl^- channels in response to a purinergic receptor. Because no purine stimulation was applied during this trial, crenation may have been unlikely to happen. Furthermore, iMOP cells were able to manage the different Ca^{2+} concentrations as their morphology was not altered.

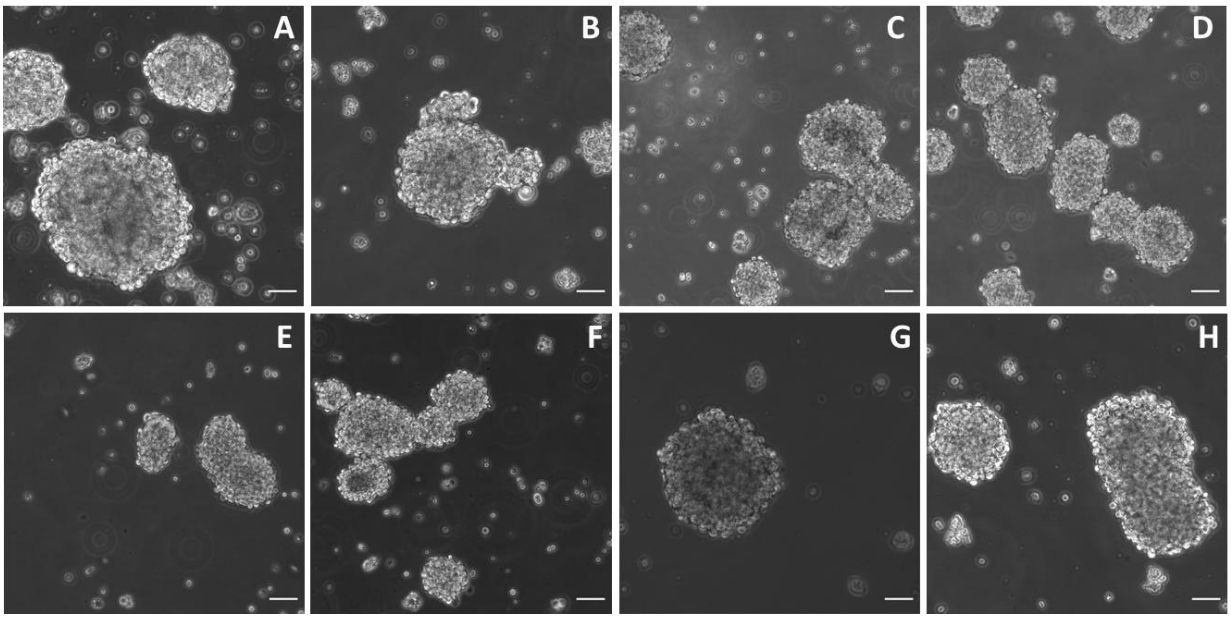

Figure 21. Micrographs of iMOP cells after 60 min under different Ca^{2+} concentrations. Control cells (A) remained in iMOP culture media and no calcium was added. Ca^{2+}[3.5 mM] (B); Ca^{2+}[2 mM] (C); Ca^{2+}[1.5 mM] (D); Ca^{2+}[1 mM] (E); Ca^{2+}[0.5 mM] (F); Ca^{2+}[0.2 mM] (G) and Ca^{2+}[0.05mM] (H). Scale bar is 50 µm.

Next, an ATP sensitivity test was performed. Adenosine triphosphate (ATP), is an agonist for both P2Y and P2X purinergic receptors. In order to evaluate if any morphological changes occurred to iMOP cells when applying ATP, different ATP concentrations solutions were proved. Two-minute videos were recorded and otospheres were analyzed by comparing their initial state with their final state. No darkening zones were seen, however, differences on otospheres sizes (total area) were observed. The change rate was calculated as $\frac{S_f}{S_i}$ (ratio between final size S_f and initial size S_i) and is presented in Figure 22. In the boxplot, the box represents the interquartile range (50% of the data). Whiskers show the minimum and maximum observed value. The dotted lines (green) are the mean and orange lines are the medians. Notches are the confidence interval around the median, if the notches in the boxplot do not overlap it can be concluded that, with 95% confidence, the medians do differ. The horizontal red line stands at 1, meaning no change between initial and final measures. For low ATP concentrations (5 µM, 500 nM, 50 nM and 5 nM) no size change was detected. Then, in medium ATP concentrations (5 mM, 500 µM and 50 µM) a slight swelling of the spheres was visible and reported as an increase of iMOP sphere size. Oppositely, at the highest ATP concentration (50 mM) a clear size decrease was noticed perhaps due to crenation. In an unexpected way, the control group, on which HBSS buffer (Ca^{2+} and Mg^{2+} free) was applied, showed growth of otospheres sizes.

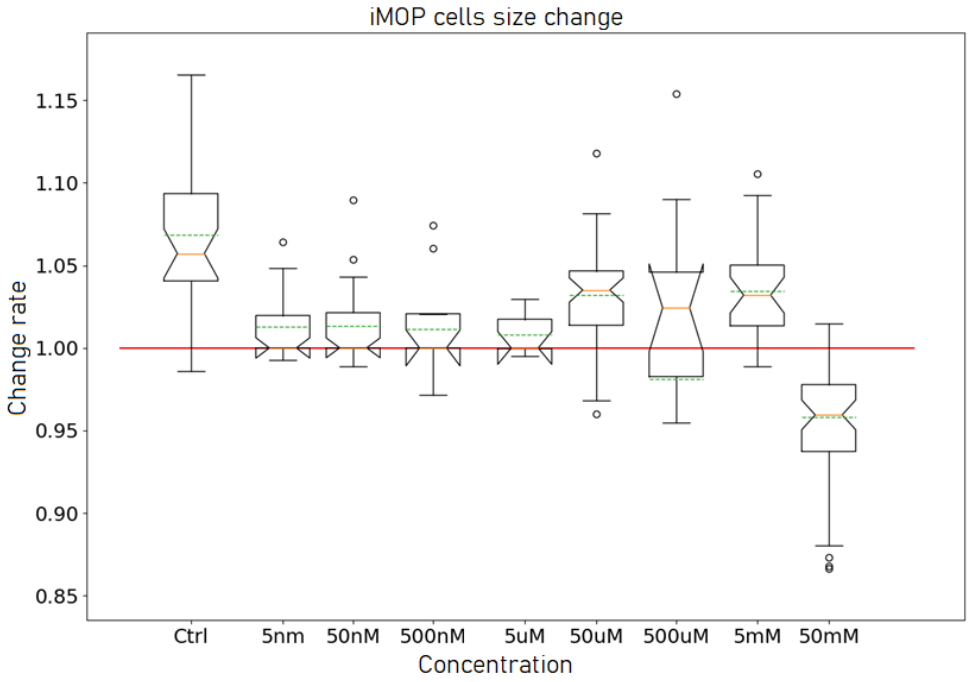

Figure 22. Notched boxplot of iMOP cells size change rate after ATP stimulation at different concentrations. Green dotted line indicates the mean while orange line indicates the median. Outliers are shown as black circles. When notches in the boxplots do not overlap, it can be concluded, with 95% confidence, that the medians do differ.

In order to measure calcium concentrations in iMOP cells, the green-fluorescent calcium indicator Fluo-4 was used. Being an AM ester, Fluo-4 should be reconstituted in anhydrous dimethyl sulfoxide (DMSO). As DMSO is considered a low toxicity solvent, it could modify iMOP cells' behavior, so a control test was performed. Fluo-4 loading protocol [119] indicates incubating the cells at 37 °C at a 1-5 µM concentration of DMSO in HBSS buffer. To observe IMOP cells' response to DMSO, the suggested incubation time was doubled. The results are shown in Figure 23. Morphology of the otospheres is not modified even after 60 minutes thus, working with the recommended loading medium should not alter iMOP cells.

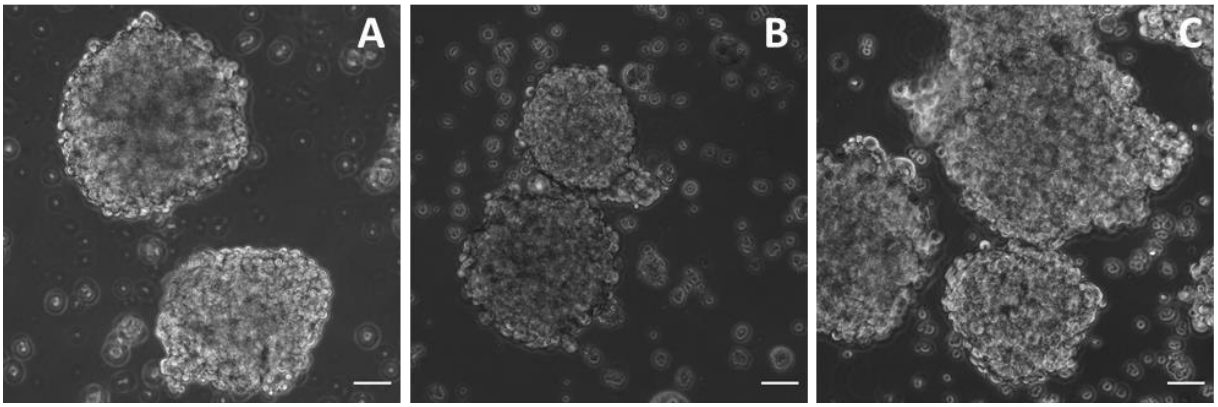

Figure 23. Micrographs of iMOP otospheres exposed to DMSO [2 µM] for 30 min (B) and 60 min (C). Control (A) was free of DMSO. Length of scale bar is 50 µm

Once control trials were performed, Ca^{2+} imaging experiments using Fluo-4 were pursued. Two-minute videos were recorded, and 8 different ATP concentrations were tested: 50 mM, 5 mM, 500 µM, 50 µM, 5 µM, 500 nM, 50 nM and 5nM considering that previous work on purinergic signaling have used a micromolar concentration [77, 120]. ATP was applied at around 10 s from the beginning of the recordings and fluorescence variation over time ($\frac{\Delta F}{F_0}$) was graphed. Graphs of three representative ATP concentrations are displayed in Figure 24: one graph belongs to the highest concentration, then a middle concentration (50 µM) and last, a low concentration (50 nM). When comparing the charts, it is evident that in 50 nM only a few peaks, not oscillatory but rather step responses are seen. In 50 mM only one peak is observed, and no oscillatory responses are detected. Differently, the middle concentration shows more oscillations through the recording. Furthermore, response curves clearly show distinct trends beyond oscillatory with high peaks and non-oscillatory. Some are step-like curves that had one positive peak and either remained steady at the highest point or returned to zero.

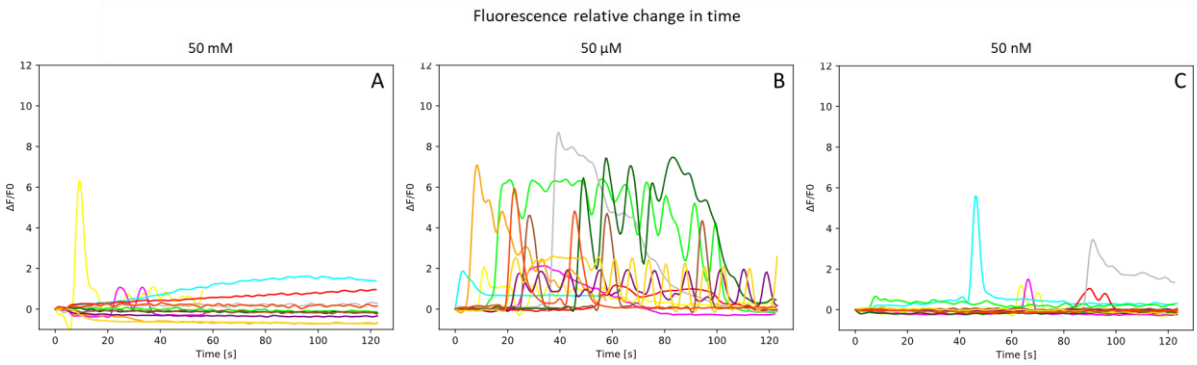

Figure 24. Representative graphs of fluorescence intensity variation over time. Stimulation of iMOP cells with three ATP concentrations: (A) 50 mM shows non-oscillatory responses; (B) 50 µM several oscillatory and step-like responses are observed and (C) 50 nM only few step-like curves were detected.

To have a clearer perspective of these results, a dose-response chart of the eight ATP concentrations used to stimulate iMOP cells was created to compile the results of the spectral analysis. A typical dose-response curve comprises a slope and a point of maximal efficacy of the measured response. However, when graphing this dose-response curve it could be seen that there is not a single slope but it rather shows an M-shaped curve where ATP 500 µM and ATP 500 nM had the highest responses (highest mean of $\frac{\Delta F}{F0}$) and both the highest and lowest concentrations had less response Figure 25.

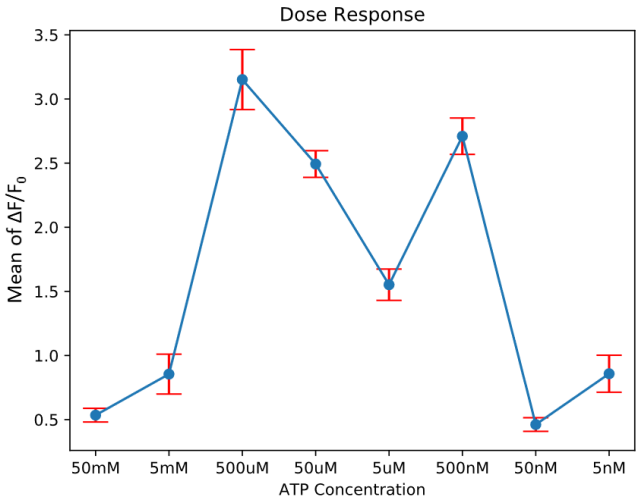

Figure 25. Dose-response relationship between the different ATP concentrations used to stimulate P2 receptors of iMOP cells. The eight ATP concentrations used on the present work are displayed according to the mean of $\frac{\Delta F}{F0}$ ± SEM, forming an M-shaped curve For 50mM n=118; 5mM n=70; 500µM n=220; 50µM n=410; 5µM n= 339; 500nM n=459; 50nM, n= 190; 5nM n=190.

In order to understand if response behavior could be related to the ATP concentrations used, graphs were further examined. According to the response's patterns in, three main trends were found at all ATP concentrations: oscillatory responses, step responses and non-oscillatory responses. In oscillatory responses (Figure 26 A) peaks were always clear and showed different frequencies and varied amplitudes. Step responses (Figure 26 B) displayed a single peak with rise time after ATP stimulation and big amplitudes sometimes not returning to zero or going back slowly showing a ramp-like trace. Non-oscillatory responses (Figure 26 C) were closer to the steady state or zero but would also have some minor peaks.

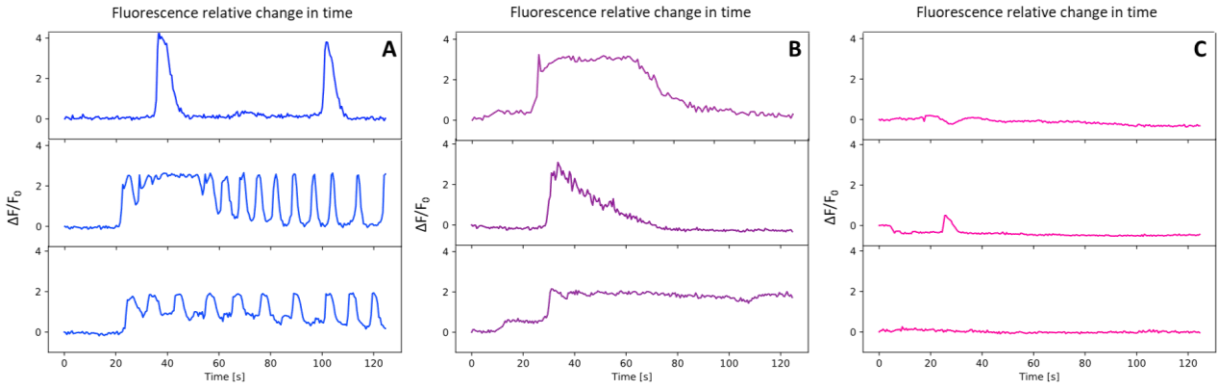

Figure 26. Classification of the different types of response to ATP. Oscillatory responses (A) showed more than one peak with varied frequencies. Step responses (B) differed more on their amplitudes. Non-oscillatory responses (C) were closer to zero and show a constant behavior. Examples taken from responses to ATP [50 µM]

Most oscillatory and step responses were present in medium ATP concentrations (500 nM, 5 µM, 50 µM, and 500 µM) shown in Figure 27 C-F. Whereas non-oscillatory responses prevailed in the lowest (50 nM -5 nM, Figure 27 B and C) and highest (50 mM, Figure 27 H) ATP concentrations. No specific amplitudes or frequencies for each concentration were observed. However, small oscillations (max. peak amplitude $\Delta F/F_0 \leq 1$) could be seen throughout all concentrations. Step responses show cells that remained in saturation perhaps because of an overload or due to excessive rising Ca^{2+} concentration which accelerates and disrupts normal metabolism leading to cell death. For the purpose of this work, step responses were not considered.

In addition to ATP responses, tests using a buffer and an ATP receptor blocker were performed. As Hank's Buffered Saline Solution (HBSS) free from Ca^{2+} and Mg^{2+} is used as solute during ATP concentrations trials, it was chosen as the buffer. On the other side, suramin has been identified as a blocker with increased potency and selectivity for P2X receptors, so it was chosen as the ATP

antagonist. Since the main responses for ATP concentrations stimulation appeared on the micromolar range, only the three middle concentrations (5 µM, 50 µM, and 500 µM) were used as controls. Stimulation of HBSS and suramin solutions followed the same protocol as when working with ATP: cells immersed in HBSS, keeping the solutions at low temperature and administered ~10 s after the start of the video.

HBSS was applied into cells as the first stimulating. As low ATP concentrations induced reduced oscillatory response, no reaction was expected in the absence of ATP. Though, somehow in an unpredictable way, some oscillatory responses were observed. As seen in Figure 28 A, 7.7% of the analyzed ROIs had an oscillatory behavior. The reason why this happens is still uncertain but the cell's activity due to mechanical stress could be considered. A thorough analysis should be performed; however, such research was not in the scope of this project.

Then, different ATP concentrations were tested on cells in the presence of an ATP antagonist. Suramin has been reported to block purinergic receptors at 200 µM [121] and so, the same concentration was used in the present work but it did not affect the ATP-stimulated cells at the highest concentration (500 µM), as oscillatory responses were detected in 10% of the analyzed ROIs while 72.5% of the total response was non-oscillatory (Figure 28 B). Yet, suramin seemed to antagonize ATP on the following lower concentrations (5 and 50 µM) as no significative oscillatory response was detected (Figure 28 C and D). Suramin's antagonism of ATP has found to be reversible, selective and competitive [122, 123, 124], meaning it does not completely blocks ATP action and the appearance of some responses could be explained. Moreover, suramin is a highly charged molecule at physiological pH and, therefore, unable to permeate the cell membrane by passive diffusion [125]. Apparent antagonist K_d values of compounds related to suramin at P2 purinoceptors are varied (between 1.18 and 10.1 µM) [126]. HBSS and suramin were applied to iMOP cells on suramin (Figure 28 E and F), and no oscillatory responses were observed. It is important to mention that the total number of experiments performed with suramin was small because the movement of the otospheres in the solution increased (probably due to suramin's high negative charge) and ROIs could not be followed.

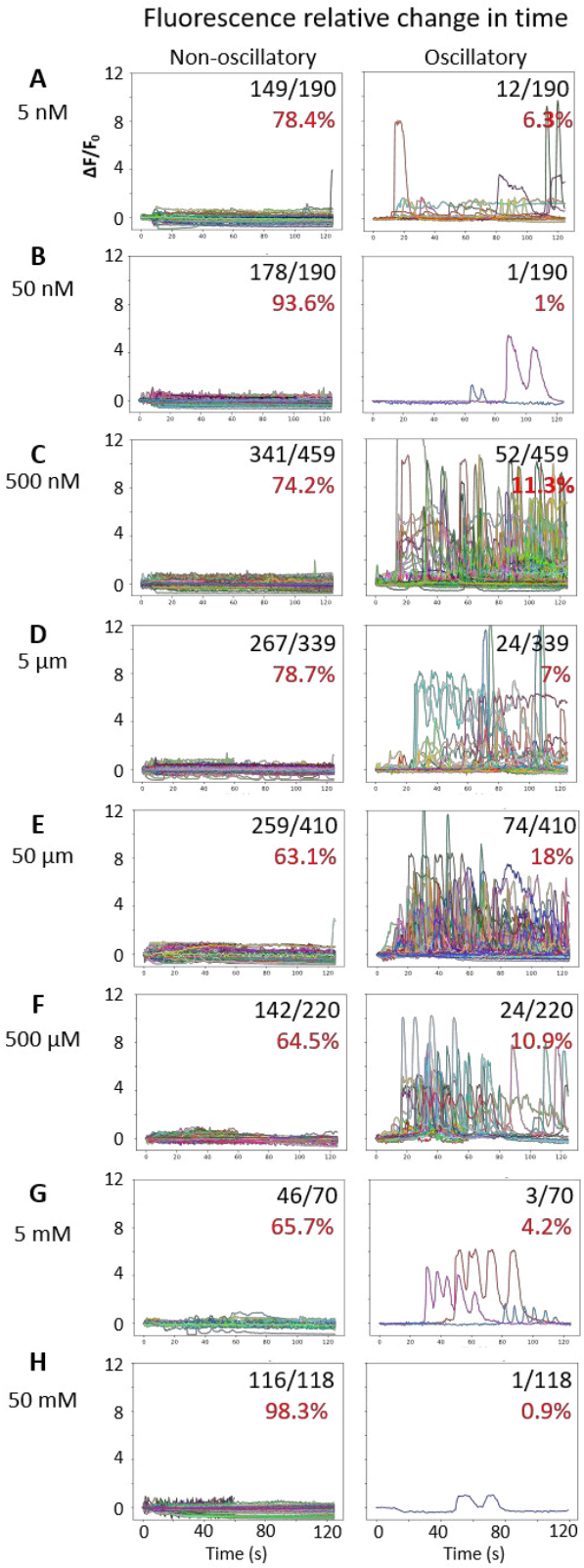

Figure 27 Intercellular Ca^{2+} signaling using Fluo-4 in iMOP cells. Eight ATP concentrations: 5 nM (A), 50 nM (B), 500 nM (C), 500 µM (D), 50 µM (E), 5 µM, (F) 50 mM (G) and 5 mM (H) were tested. Graphs were classified depending on their response into oscillatory or non-oscillatory. Number of response ROIs / Total number of ROIs are shown in black inside the graphs followed by the equivalent percentage in red. Missing values correspond to step responses.

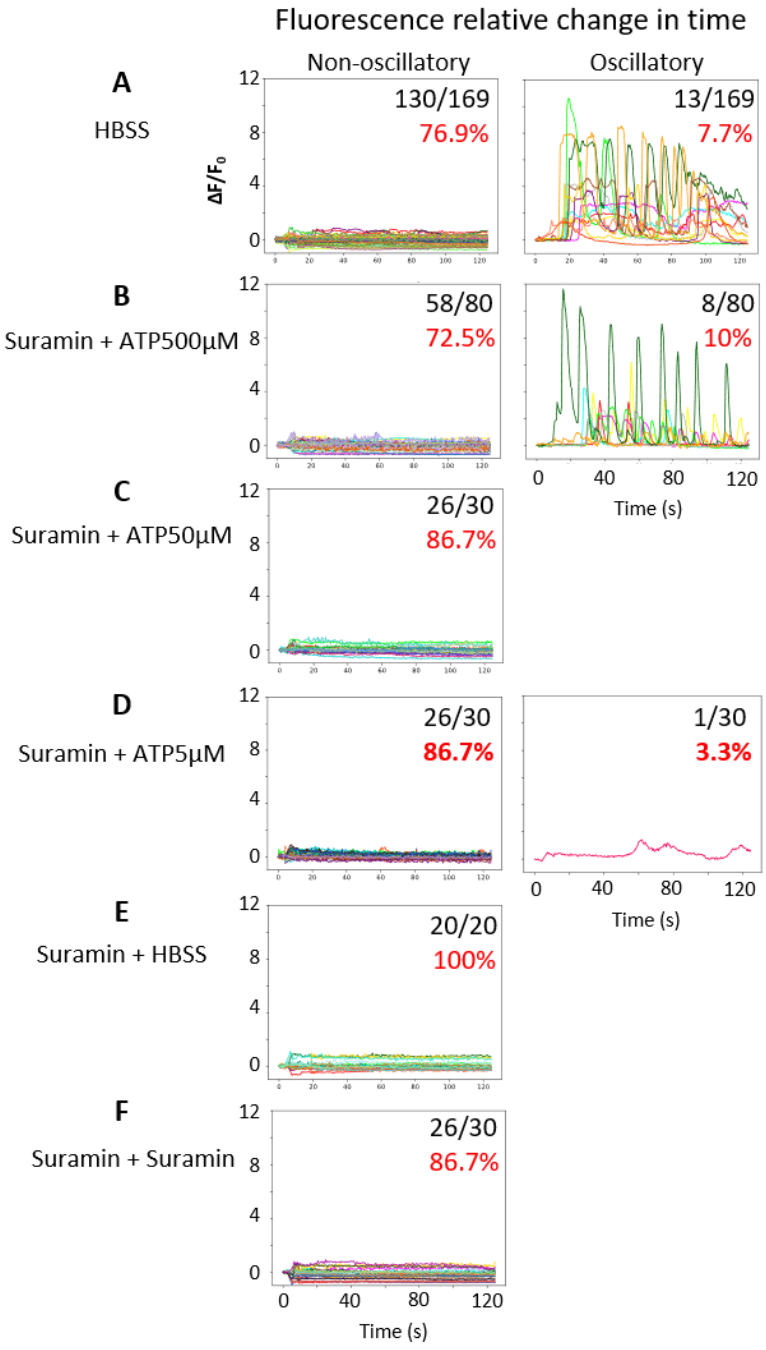

Figure 28 Intercellular Ca^{2+} signaling using Fluo-4 in iMOP cells. As controls, HBSS (A) and Suramin 200 µM were tested. For cells in suramin, 3 ATP concentrations were tested: 5 µM (B), 50 µM (C) and 500 µM (D). HBSS (E) and Suramin (F) were also investigated as negative controls. Graphs were classified depending on their response into oscillatory or non-oscillatory. Number of response ROIs / Total number of ROIs are shown in black inside the graphs followed by the equivalent percentage in red. Missing values correspond to step

As an alternative analysis, frequencies of the oscillatory responses were analyzed in detail to obtain insight about the cell's behavior. To achieve this, data without stimulation (resting state) was needed as a control. Baseline was generated by recording two minutes of Fluo-4 loaded iMOP cells, ROIs were analyzed in the same way as the previous ones when using ATP. Figure 29 shows that spontaneous peak responses can also be found. This could mean that the otospheres are in good condition as there is some sporadic efflux of $[Ca^{2+}]_I$ produced by the endoplasmic reticulum due to the physiological activity of the cells.

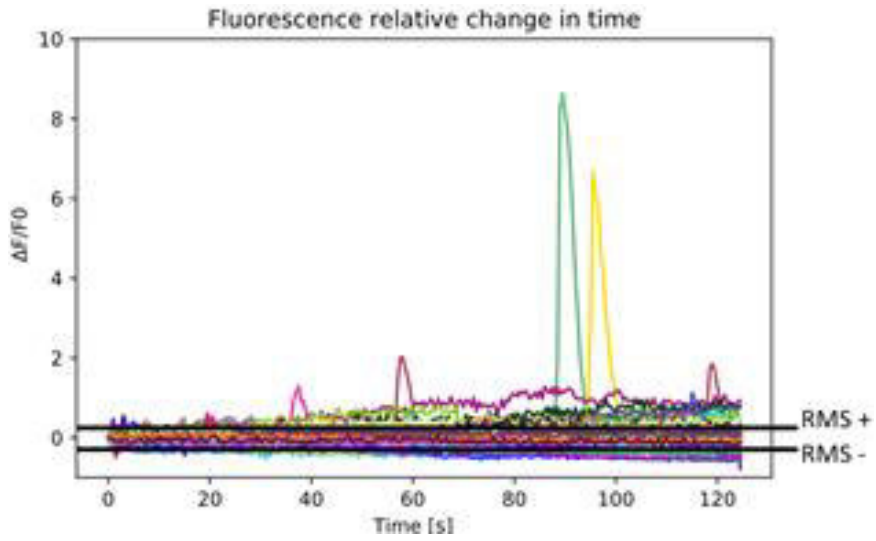

Figure 29. iMOP cells baseline temporal curve of the relative fluorescence intensity change. Two-minute videos of otospheres previously loaded with Fluo-4 without any stimulation were recorded and analyzed. The RMS of this data was calculated and is indicated on the image (RMS = ±0.15)

Having an identified baseline behavior, a point from which data could be considered either responsive or non-responsive to stimulation could be established. To achieve this, the root mean square (RMS) of the baseline was calculated and it is indicated in Figure 29. Data values above RMS = +0.15 were considered as responsive and on the contrary, data with smaller oscillations were considered as non-responsive. Data below RMS = -0.15 were discarded. ROIs data from all experiments were then classified according to this new parameter.

In order to obtain insight into the response classification, a spectral analysis was performed in the responses which were reclassified taking in consideration the RMS. For the spectral analysis, a Fourier transform was performed to convert a time function (time domain) into a sum or an integral of sine waves of different frequencies (frequency domain). In order to understand the output, a sine function of known frequency was computed and its FFT was calculated. A power spectral density plot and a

frequency histogram were obtained from the analysis program. Figure 30 A and B shows a sinusoidal function *g(t)* in the time domain and the corresponding power spectrum and frequency histogram. In the frequency domain, the PSD results in one dominant peak of frequency 33 mHz which reflects the period of the function (t = 30 s).

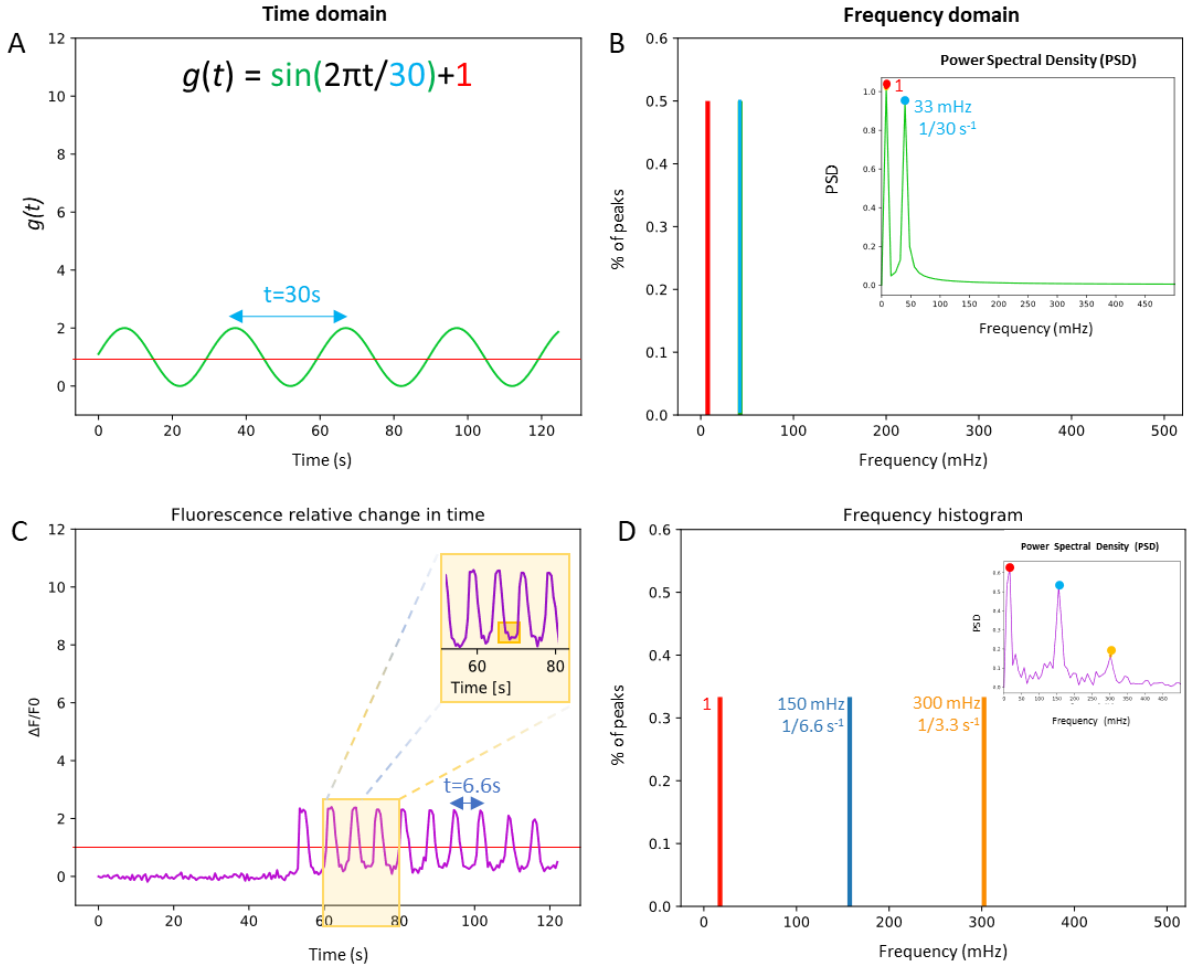

Figure 30. A sinusoidal function *g(t)* (A) and a Ca^{2+} recording showing one oscillating ROI in the time domain (C), and their corresponding frequency histogram and PSD in the frequency domain (B and D). The frequency of *g(t)* is 33 mHz, which is equal to a periodicity (t) of 30 s (A and B). The periodicity (t) of the Ca^{2+} oscillation is 6.6 s, which is equal to a frequency of 150 mHz. This value can be observed as a prominent peak in the frequency domain (blue dot) and is indicated with a blue bar on the histogram. Another peak with a lower relative power is observed in the spectrum with a t= 3.3 s and a 300 mHz frequency, indicated in orange (C and D).

The peak that corresponds to the constant term is indicated in red. The frequency histogram shows the percentage of peaks for each frequency, in this case: 50% of the peaks are at 1 mHz and 50% at 33 mHz.

Figure 30 C and D shows a spectral analysis of an actual Ca^{2+} recording of a single ROI with varied frequencies. The output after FFT, shows a PSD with three peaks reflecting different frequencies (300

mHz, 150 mHz and the constant at 1 mHz) of the Ca^{2+} response. In the PSD, the constant frequency is shown with a red dot, the next frequency with dominant amplitude can be observed at 150 mHz (blue dot) and finally, a smaller peak is shown in 300 mHz (orange dot). The highest frequency was found out to be due signal noise on the valleys of the signal, a close up in Figure 30 C shows its short periodicity. On the frequency histogram (Figure 30 D), each bar corresponds to the frequency with the same color as in the PSD. It is observed that the percentage of peaks that correspond to each frequency is the same (33%).

With this analysis, it could be concluded that there is a range of frequencies where responses can be considered as relevant. Namely, the constant frequency appears on every frequency histogram and high frequencies are related to noisy signals. Taking this into consideration, it was decided that an adequate interval where significant frequencies could be found is between 30 mHz – 250 mHz.

Once the baseline and the frequencies range were established, the spectral analysis was performed in the ATP-evoked Ca^{2+} recordings. Results are shown in Figure 31 and Figure 32, where frequency histograms were arranged as negative (non-oscillatory or oscillations below RMS) or positive (oscillations above the RMS). Frequencies below 30 mHz are shown in gray and the percentage of ROIs for each concentration is displayed in red in the upper right corner of each histogram. Missing data correspond to step and discarded responses. The baseline is shown in (Figure 32 F), most of the peaks are low frequencies being 100 mHz the highest frequency where peaks appear.

There is little frequency variation at low concentrations, ATP 50 and 5 nM, but high frequencies of up to 225 mHz can be seen on the positive responses. For the negative responses, small peaks at frequencies lower than 150 mHz were found (Figure 31 A and B). In the medium concentrations, ATP 500 µM, 50 µM, 5 µM and 500 nM, a greater variety of frequencies was found on the positive responses with peaks of up to 225 mHz. Negative responses were in the same frequencies range but with a lower percentage of peaks (Figure 31 C-F). For the highest concentrations, ATP 50 and 5 mM (Figure 31 H and I), the frequencies of the positive responses appeared in a few specific low frequencies of up to 160 mHz but with a large percentage (70%) on frequencies below 50 mHz. Negative responses were mainly low frequencies.

Experiments using HBSS and suramin are shown in Figure 32. In the HBSS histogram (Figure 32 A), most positive response peaks are concentrated in low frequencies although some peaks around 170 mHz are present. Negative responses peaks are mainly around 50 mHz or less. In the histogram of iMOP cells in

suramin to which ATP 500 µM was added (Figure 32 B), small peaks (~5%) at varied frequencies up to 150 mHz are shown on positive responses. Less variety of frequencies is shown with the negative responses, where frequencies lower than 100 mHz are seen. In histograms of otospheres in suramin with the addition of smaller ATP concentration (ATP 50 and 5 µM), a similar behavior is shown. Both positive and negative responses are at frequencies below 100 mHz and negative responses under 25 mHz (Figure 32 C and D). On the histogram displaying suramin + HBSS calcium signaling responses, both positive and negative responses react below 50 mHz (Figure 32 E). On the frequency histogram showing data of suramin + suramin (Figure 32 G) experiments, there were only positive responses not greater than 50 mHz.

When observing the spectral analysis, histograms do not exhibit a pattern that can help differentiate between the different ATP concentrations. But, as an interesting fact, it is observed that in negative responses a large percentage of peaks is found on low frequencies, similar to the baseline. While more peaks in higher frequencies are seen with positive responses. The use of the P2X purinoceptor antagonist, suramin [200 µM] does not inhibit ATP [500 µM]-induced flux completely but seems to antagonize receptor activation with lower ATP concentrations. Suramin has been reported to differ its potency to block at the rat, mouse and human receptors [127, 128] by a single amino acid difference. The rat receptor has glutamine at position 78 and is relatively insensitive to suramin; the human receptor has lysine and is more readily blocked. The mouse receptor has glutamine in this position; ATP-evoked currents in this position are increased by concentrations of suramin (3-100 µM) that block other P2X receptors [129] or are unaffected [130, 131].

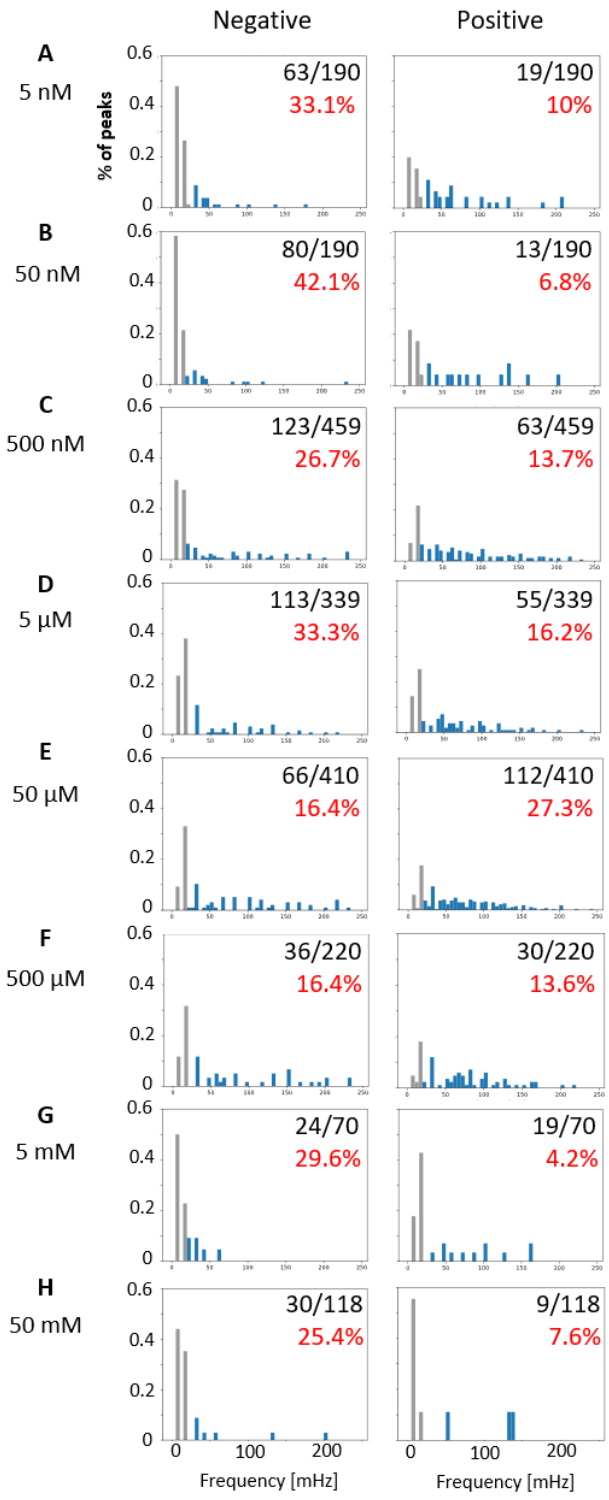

Figure 31. Frequency distribution histograms of calcium responses to ATP. *Negative* refers to responses either non-oscillatory or below the RMS, while *Positive* indicates oscillatory responses above RMS value. Columns in gray in each histogram indicate frequencies < 30 mHz. Eight ATP concentrations: 5 nM (A), 50 nM (B), 500 nM (C), 5 µM (D), 50 µM (E), 500 µM, (F) 5 mM (G) and 50 mM (H) were tested. Number of responsive *ROIs / Total number of ROIs* are shown in black inside the graphs followed by the equivalent percentage in red. Missing values correspond to step and discarded responses.

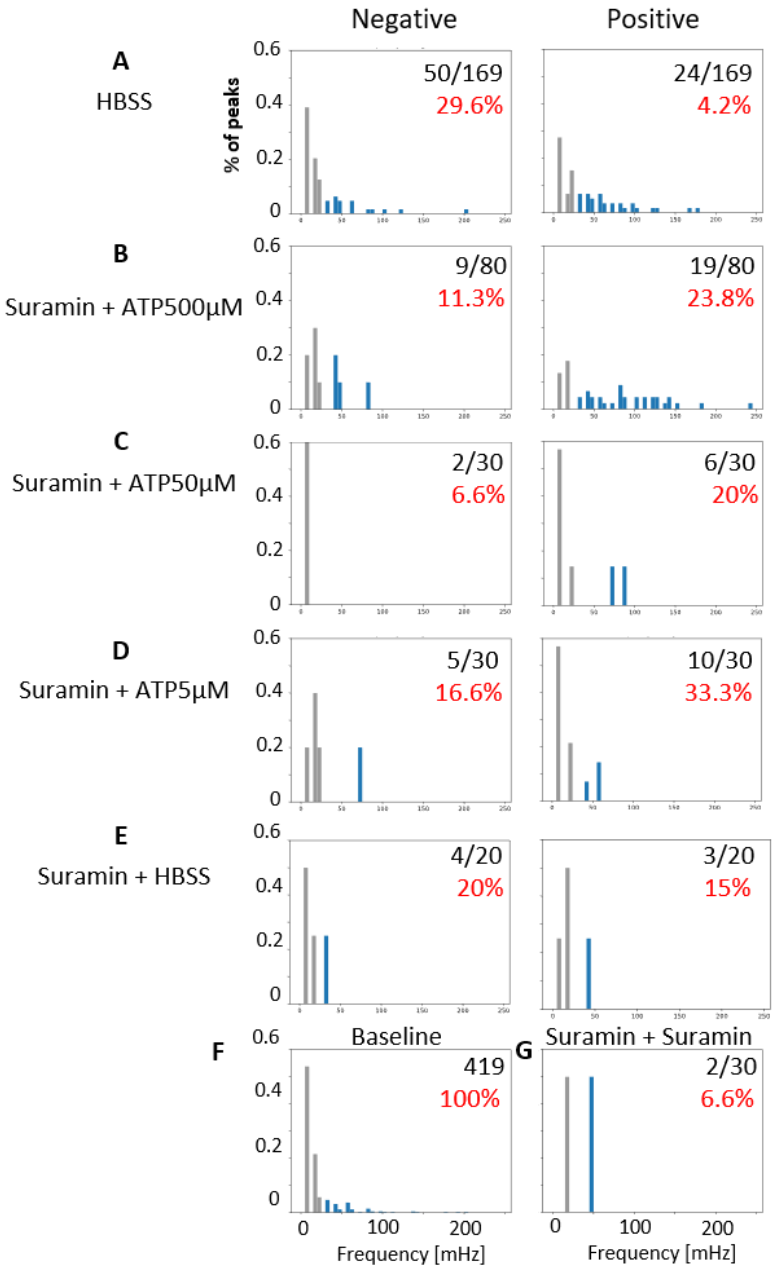

Figure 32 Frequency distribution histograms of calcium responses to HBSS and Suramin. *Negative* refers to responses either non-oscillatory or below the RMS, while *Positive* indicates oscillatory responses above RMS value. Columns in gray in each histogram indicate frequencies < 30 mHz. As controls, HBSS (A) and suramin were tested. For cells in suramin, 3 ATP concentrations were tested: 500 µM (B), 50 µM (C) and 5 µM (D). HBSS (E) and suramin (G) were also investigated as negative controls. Baseline frequencies distribution is shown in F. Number of responsive *ROIs / Total number of ROIs* are shown in black inside the graphs followed by the equivalent percentage in red. Missing values correspond to step and discarded responses

6. DISCUSSION AND CONCLUSIONS

The main aim of the present work was to determine the presence of purinoceptors in a fate restricted immortalized multipotent otic progenitor (iMOP) cell line. Purinergic signaling is present from the earliest developmental stages as a mediator of particular physiological functions at different stages of development or to control the developmental processes themselves [96, 104, 132]. Since the embryonic stage, P2X receptors have shown to be involved in the development and regulation of auditory and vestibular sensory transduction [104]; in the development of afferent and efferent innervation of the sensory hair cells [133]; and in the cochlea synaptic reorganization and establishment of neurotransmission prior to the onset of hearing function [87, 134]. In the late embryonic period, P2Y receptors were found in cells lining the cochlea partition associated with the electrochemical environment that provides the driving force for sound transduction [88]. P2X and P2Y receptors were found to mediate spontaneous electrical potentials in Köllicker's organ cells by spontaneous release of ATP via connexin hemichannels [42, 89]. And, in the developed cochlea, hemichannel-mediated ATP release may be important in regulating the electromotility of the outer hair cells [91, 135] and have also been shown to be implicated in acoustic trauma events [77, 136, 120].

Most of these studies have been performed on embryos and tissue, however, since purinergic signaling was shown to be involved in stem cell development, including regulation of proliferation, differentiation and cell death, there is a growing interest in this research area [85, 104]. Despite this, mouse embryonic stem cells and induced pluripotent stem cells have been studied to obtain hair cell-like cells for replacement therapies [137, 138] but purinergic signaling remains uncharacterized in stem cells derived from the cochlear progenitors. Since iMOP cell culture was initiated, it enabled the study of purinoceptors through calcium signaling which in turn will allow the study of diverse cellular processes that are dependent on Ca^{2+} signaling (cell motility, exocytosis, etc.).

Research about purinergic signaling in stem cells is relatively recent and thus there are only a few papers about this topic. The present work is a pioneer in the investigation of the existence of purinergic receptors in otic progenitor cells, and to our knowledge, the first one in iMOP cells. It represents a reference that has laid the foundations in one way in which floating otospheres can be handled for calcium signaling imaging. Being the first work with iMOP cells, we faced several challenges. One of the challenges was to handle the spheres for their visualization at the microscope, which was solved by

using drilled culture dishes. Then, we dealt with the turbulence generated after manual application of ATP by deletion and interpolation of the images. To properly analyze the floating cells, manual tracking was needed so a new computing program was created. Due to its three-dimensional nature, selecting single cells in the same focal plane was not easy and therefore in the program the cells are segmented by hand (regions of interest) allowing a proper relative fluorescence change analysis. Lastly, as heterogeneous responses where observed, that is, responses that were not clearly correlated to ATP stimulation, a spectral analysis was proposed.

The key finding of our study was that iMOP cell line, in its undifferentiated state, already expressed purinergic P2 receptors coupled to Ca^{2+} signaling. An ATP-induced increase in intracellular calcium levels was seen in calcium-free medium while P2 antagonist suramin mostly inhibited the increase, thus suggesting that the calcium elevations are due to a release from the calcium store after activation of phospholipase C [139]. Particularly, it has been reported that coupled to phospholipase Cγ, P2Y2 triggers calcium release from intracellular stores via IP3 in human mesenchymal stem cells (hMSC) [139]. The calcium wave in these cells would be then propagated due to the elevated, free cytosolic calcium, which leads to the release of ATP that binds to P2 receptors of adjacent cells. In the present work, calcium imaging showed that P2 receptors mediate Ca^{2+} signals in iMOP cells and that P2Y receptors most likely activate the PLC-IP3 pathway and release Ca^{2+} from internal stores. A propagation of the calcium signal similar to the calcium waves in hMSC was observed in some cases in iMOP otospheres but the corresponding analysis was not performed as it was not the purpose of this work.

The importance of purinergic signaling in stem cell biology includes regulation of proliferation, migration, differentiation and cell death of multipotent stem cells [104, 96]. Hence, the ATP-mediated responses in iMOP cells might be involved in signals to modulate these processes in the otospheres. Moreover, purinergic receptors interact with a variety of growth factors and neurotransmitter receptors, which may modulate ATP-induced responses [140]. So far, only few data are available in the literature on the role of P2 receptor activation in stem and progenitor cells. The present work contributes to purinergic signaling research more specifically in otic progenitors. The experiments described here were performed in the absence of calcium, further work to confirm our hypothesis should consider the use of a calcium chelator such as EGTA to ensure total absence of extracellular Ca^{2+}, as well as the use of more P2 agonists (ADP, nucleotides or pyrimidines) and more antagonists (PPADS, TNP-ATP, etc.) would allow us to perform a cross-study that provides detailed information in order to determine which purinoceptors are present and functional in the otospheres.

An important point to consider when working with cultured cells is their physiological state on experimentation days. For example, response variation (either positive, negative or step response) could be due to performing several repetitions on increasing passage number cultures and varied number of otospheres at the time of performing the experiments. It is also relevant to consider that temperature at the time of performing the experiments, and the mechanical stimulation caused by the fall of the drop may result in receptor activation. Particularly, it could be considered whether mechanically activated ion channels exist in iMOP otospheres. Piezo1 and Piezo2 are two members of a novel class of pressure-activated ion channels expressed by mammalian cells [141] and particularly by brain-derived human neural stem/progenitor cells [142]. The Piezo1 channel exhibits a preference for calcium in response to stimulation by static pressure, shear stress (fluid flow), and membrane stretch [143, 144, 145]. The presence of activity of this receptor should be considered and properly proved, for example, by using specific drugs like the pharmacological inhibitor GsMTx-4 [142] to see if Piezo 1 could play a role in our Ca^{2+} signaling experiments.

More importantly, recent personal communication with Dr. Kwan (responsible for iMOP cells generation) has led us know that his working group has recently initiated single cell RNA sequencing to decipher the heterogeneity in cell types in undifferentiated iMOP cells. Results from this study could lead us to a pathway in which each cell that conforms an otosphere is different one from another (in which case, it is important to know which and how many different cell types there are) and could explain the different responses of P2 purinoceptors activation when applying ATP in our experiments (response or lack of response, amplitude and frequency of the response).

Furthermore, one of the achievements of this work was to establish a program that allows a frame by frame analysis of the experiments. A search was made to find software that allows a follow-up analysis of the otospheres. However, no program that could identify the same sphere over time and would do a fluorescence relative change in time analysis was found. The program established in the present work allows the user to individually track a sphere frame-by-frame and discard turbulent images. Further work should additionally consider replicating all the performed and suggested tests on differentiated cells to investigate if purinoceptors expression is dependent on the developmental stage and if the receptors are associated with a specific type of cell.

As an original proposal, a spectral analysis where time domain information is transformed into information in the frequency domain was performed in the present work. Although spectral analysis does not provide a specific pattern depending on ATP concentration, a frequency range in which the

responses can be associated with the stimulus was found. There are bands in the frequency spectrum that are present at certain concentrations that may be associated with the activity of the cells due to ATP stimulation. For example, in medium concentrations (500 nM, 5 µM, 50 µM, 500 µM) where positive responses exist in greater percentage, frequencies around 75-150 mHz are more abundant than in greater (5 mM and 50 mM) or minor (50 nM and 5 nM) ATP concentrations. It is proposed to focus on these specific regions of the spectrum by modifying the parameters of the program (binarization, filtering, relative power that determines a peak) to accurately detect if there is a direct correlation between the stimulus and a specific frequency. The analysis to corroborate the correlation would be done once as many external factors as possible (like Ca^{2+} absence, temperature and mechanical activation control) are resolved.

Briefly, according to the established objectives for this work, it can be concluded that:

1. P2 purinergic receptors presence was identified in iMOP cells after ATP stimulation. This finding is one of the firsts reports about purinergic activity in otic stem cells.
2. No adverse effects due to the use of compounds used during calcium signaling experiments were observed.
3. An accurate classification of the responses to ATP stimulation by means of a spectral analysis could not be established, however, a trend associated with high and low frequencies at different ATP concentrations could be observed.

Moreover, the program generated in this work has enabled the reported results and will facilitate future experiments of our group.

As future work, the use of a calcium chelator and more P2 agonists and antagonists must be performed to confirm the presence of P2 purinoceptors. It will also be important to determine the existence of mechanically activated ion channels such as Piezo 1 in iMOP otospheres. Additionally, to investigate purinoceptors expression on different developmental stages, the same tests must be replicated in differentiated iMOP cells. And finally, to improve the spectral analysis and make a more accurate correlation between the stimulus and a specific frequency, external factors that are now interfering with the analysis should be resolved.

REFERENCES

[1] L. M. Gil-Carcedo, Otología, Editorial Médica Panamericana, 2011.

[2] J. E. Hawkins, "Encyclopædia Britannica," Encyclopædia Britannica, inc., 21 July 2017. [Online]. Available: https://www.britannica.com/science/ear. [Accessed 31 March 2018].

[3] B. Higashida Hirose, Ciencias de la salud, Séptima edición ed., México, D.F.: McGraw Hill Education, 2013, pp. 117-120.

[4] A. R. Møller, Hearing : anatomy, physiology, and disorders of the auditory system, Second Edition ed., Burlington, MA, USA: Elsevier Inc., 2006.

[5] I. Tasaki and C. S. Spyropoulos, "Stria vascularis as source of endocochlear potential," *Journal of Neurophysiology,* vol. 22, no. 2, pp. 149-155, 1959.

[6] A. J. Hudspeth, "The Cellular Basis of Hearing: The Biophysics of Hair Cells," *Science,* vol. 230, no. 4727, pp. 745-752, 15 November 1985.

[7] Biology Boom Copyright ©, "https://biologyboom.com," [Online]. Available: https://biologyboom.com/describe-the-structure-of-human-ear-give-a-summary-of-process-of-hearing-and-equilibrium-in-man/. [Accessed 8 Octubre 2018].

[8] E. R. Kandel, J. H. Schwartz and T. M. Jessell, Principles of neural science, 4th edition ed., New York: McGraw-Hill, Health Professions Division, 2000.

[9] J. Zheng, . W. Shen, D. Z. He, K. B. Long, L. D. Madison and P. Dallos, "Prestin is the motor protein of cochlear outer hair cells," *Nature,* vol. 405, no. 6783, pp. 149-155, 11 May 2000.

[10] A. W. Peng, F. T. Salles, B. Pan and A. J. Ricci, "Integrating the biophysical and molecular mechanisms of auditory hair cell mechanotransduction," *Nature Communications,* vol. 2, no. 523, pp. 1-14, 1 November 2011.

[11] D. Purves, G. J. Augustine, D. Fitzpatrick, W. C. Hall, A.-S. LaMantia, J. O. McNamara and S. M. Williams, "Hair Cells and the Mechanoelectrical Transduction of Sound Waves," in *Neuroscience*, Third ed., Sunderland, MA, Sinauer Associates, Inc., 2004, pp. 283-313.

[12] R. Gueta, E. Tal, Y. Silberberg and I. Rousso, "The 3D structure of the tectorial membrane determined by second-harmonic imaging microscopy," *Journal os Structural Biology,* vol. 159, no. 1, pp. 103-110, 2007.

[13] J. O. Pickles, in *An introduction to the physiology of hearing*, Fourth edition ed., Bingley, Emerald, 2012, pp. 28-33.

[14] R. Fettiplace, "Hair cell transduction, tuning, and synaptic transmission in the mammalian cochlea," *Comprehensive Physiology,* vol. 7, no. 4, pp. 1197-1227, 2017.

[15] K. F. Barald and M. W. Kelley, "From placode to polarization: new tune in inner ear development," *Development,* vol. 131, no. 17, pp. 4119-4130, 2004.

[16] Z. F. Mann and M. W. Kelley, "Development of the inner ear," in *Principles of developmental genetics*, Second ed., S. A. Moody, Ed., Academic Press, 2014, pp. 377-387.

[17] M. M. Riccomagno, S. Takada and D. J. Epstein, "Wnt-dependent regulation of inner ear morphogenesis is balanced by the opposing and supporting roles of Shh," *Genes & development,* vol. 19, no. 13, pp. 1612-1623, 2005.

[18] T. Ohyama, O. A. Mohamed, M. M. Taketo, D. Dufort and A. K. Groves, "Wnt signals mediate a fate decision between otic placode and epidermis," *Development,* vol. 133, no. 5, pp. 865-875, 2006.

[19] A. S. Brown and D. J. Epstein, "Otic ablation of smoothened reveals direct and indirect requirements for Hedgehog signaling in inner ear development," *Development,* vol. 138, no. 18, pp. 1-10, 2011.

[20] T. Okano and M. W. Kelley, "Stem Cell Therapy for the Inner Ear: Recent Advances and Future Directions," *Trends in Amplification,* vol. 16, no. 1, pp. 4-18, March 2012.

[21] A. Doetzlhofer, P. White, Y.-S. Lee, A. Groves and N. Segil, "Prospective identification and purification of hair cell and supporting cell progenitors from the embryonic cochlea," *Brain research,* vol. 1091, no. 1, pp. 282-288, 2006.

[22] R. J. Ruben, "Development of the inner ear of the mouse: a radioautographic study of terminal mitoses," *Acta Otolaryngologica (Stockholm),* vol. 220, pp. 1-44, 1967.

[23] V. Matei, S. Pauley, S. Kaing, D. Rowitch, K. W. Beisel, K. Morris, F. Feng, K. Jones, J. Lee and B. Fritzsch, "Smaller inner ear sensory epithelia in Neurog1 null mice are related to earlier hair cell cycle exit," *Developmental Dynamics,* vol. 234, no. 3, pp. 633-650, 2005.

[24] T. Yang, J. Kersigo, I. Jahan, N. Pan and B. Fritzsch, "The molecular basis of making spiral ganglion neurons and connecting them to hair cells of the organ of Corti," *Hearing Research,* vol. 278, no. 1-2, pp. 21-33, 2011.

[25] D. J. Lim and M. Anniko, "Developmental Morphology of the Mouse Inner Ear: A scanning electron microscopic observation," *Acta Oto-Laryngologica,* vol. 99, pp. 5-69, 1985.

[26] M. W. Kelley, "Cellular commitment and differentiation in the organ of Corti," *International Journal of Developmental Biology,* vol. 51, no. 6-7, pp. 571-583, 1 September 2007.

[27] G. Ehret, "Development of hearing and response behavior to sound stimuli: behavioral studies," in *Development of auditory and vestibular systems,*, R. Romand, Ed., New York, Academic Press, 1983, pp. 211-237.

[28] J. Bryant, R. J. Goodyear and R. G. P., "Sensory organ development in the inner ear: molecular and cellular mechanisms," *British Medical Bulletin,* vol. 63, no. 1, pp. 39-57, 2002.

[29] B. Fritzsch, N. Pan, I. Jahan and K. L. Elliott, "Inner ear development: building a spiral ganglion and an organ of Corti out of unspecified ectoderm," *Cell and tissue research,* vol. 361, no. 1, pp. 7-24, 2015.

[30] M. L. Basch, R. M. Brown, H.-I. Jen and A. K. Groves, "Where hearing starts: the development of the mammalian cochlea," *Journal of Anatomy,* vol. 228, no. 2, pp. 233-254, 2016.

[31] R. Gu, R. M. Brown, C.-W. Hsu, T. Cai, A. L. Crowder, V. G. Piazza, T. J. Vadakkan, M. E. Dickinson and A. K. Groves, "Lineage tracing of Sox2-expressing progenitor cells in the mouse inner ear reveals a broad contribution to non-sensory tissues and insights into the origin of the organ of Corti," *Developmental Biology,* vol. 414, no. 1, pp. 72-84, 2016.

[32] M. L. Basch, T. Ohyama, N. Segil and A. K. Groves, "Canonical Notch Signaling Is Not Necessary for Prosensory Induction in the Mouse Cochlea: Insights from a Conditional Mutant of RBPjκ," *Journal of Neuroscience,* vol. 31, no. 22, pp. 8046-8058, 2011.

[33] A. E. Kiernan, A. L. Pelling, K. K. Leung, A. S. Tang, D. M. Bell, C. Tease, R. Lovell-Badge, K. P. Steel and K. S. Cheah, "Sox2 is required for sensory organ development in the mammalian inner ear," *Nature,* vol. 434, no. 7036, pp. 1031-1035, 2005.

[34] T. Ohyama, M. L. Basch, Y. Mishina, K. M. Lyons, N. Segil and A. K. Groves, "BMP Signaling Is Necessary for Patterning the Sensory and Nonsensory Regions of the Developing Mammalian Cochlea," *Journal of Neuroscience,* vol. 30, no. 45, pp. 15044-15051, 2010.

[35] H. Morsli, D. Choo, A. Ryan, R. Johnson and D. K. Wu, "Development of the Mouse Inner Ear and Origin of Its Sensory Organs," *Journal of Neuroscience,* vol. 18, no. 9, pp. 3327-3335, 1998.

[36] L. D. Urness, X. Wang, S. Shibata, T. Ohyama and S. L. Mansour, "Fgf10 is required for specification of non-sensory regions of the cochlear epithelium," *Developmental Biology,* vol. 400, no. 1, pp. 59-71, 2015.

[37] M. L. Basch, R. M. Brown II, H.-I. Jen and A. K. Groves, "Where hearing starts: the development of the mammalian cochlea," *Journal of Anatomy,* vol. 228, no. 2, pp. 233-254, 2016.

[38] M. W. Kelley, "Regulation of cell fate in the sensory epithelia of the inner ear," *Nature Reviews Neuroscience,* vol. 7, no. 1, pp. 837-849, 2006.

[39] Y.-S. Lee, F. Liu and N. Segil, "A morphogenetic wave of p27Kip1 transcription directs cell cycle exit during organ of Corti development," *Development,* vol. 133, no. 15, pp. 2817-2826, 2006.

[40] H. Laine, A. Doetzlhofer, J. Mantela, J. Ylikoski, M. Laiho, M. F. Roussel, N. Segil and U. Pirvola, "p19Ink4d and p21Cip1 Collaborate to Maintain the Postmitotic State of Auditory Hair Cells,

Their Codeletion Leading to DNA Damage and p53-Mediated Apoptosis," *Journal of Neuroscience,* vol. 27, no. 6, pp. 1434-1444, 2007.

[41] T. Schimmang and U. Pirvola, "Coupling the cell cycle to development and regeneration of the inner ear," *Seminars in Cell & Developmental Biology,* vol. 24, no. 5, pp. 507-513, 2013.

[42] N. X. Tritsch, E. Yi, J. E. Gale, E. Glowatzki and D. E. Bergles, "The origin of spontaneous activity in the developing auditory system," *Nature,* vol. 450, no. 7166, pp. 50-55, 2007.

[43] C. Woods, M. Montcouquiol and M. Kelley, "Math1 regulates development of the sensory epithelium in the mammalian cochlea," *Nature neuroscience,* vol. 7, no. 12, pp. 1310-1318, 2004.

[44] M. Ebeid, P. Sripal, J. Pecka, K. W. Beisel, K. Kwan and G. A. Soukup, "Transcriptome-wide comparison of the impact of Atoh1 and miR-183 family on pluripotent stem cells and multipotent otic progenitor cells," *PLoS ONE,* vol. 12, no. 7, pp. 1-23, 2017.

[45] B. J. Kopecky, I. Jahan and B. Fritzsch, "Correct Timing of Proliferation and Differentiation is Necessary for Normal Inner Ear Development and Auditory Hair Cell Viability," *Developmental Dynamics,* vol. 242, no. 2, pp. 132-147, 2013.

[46] K. Liu, B. Lin, M. Zhao, X. Yang, M. Chen, A. Gao, F. Liu, J. Que and X. Lan, "The multiple roles for Sox2 in stem cell maintenance and tumorigenesis," *Cellular Signalling,* vol. 25, no. 5, pp. 1264-1271, 2013.

[47] E. M. Abdelalim, M. M. Emara and P. R. Kolatkar, "The SOX transcription factors as key players in pluripotent stem cells," *Stem Cells and Development,* vol. 23, no. 22, pp. 2687-2699, 2014.

[48] M. W. Kelley, E. C. Driver and C. Puligilla, "Regulation of cell fate and patterning in the developing mammalian cochlea," *Current opinion in otolaryngology & head and neck surgery,* vol. 17, no. 5, pp. 381-387, 2009.

[49] A. Dabdoub, C. Puligilla, J. M. Jones, B. Fritzsch, K. S. E. Cheah, L. H. Pevny and M. W. Kelley, "Sox2 signaling in prosensory domain specification and subsequent hair cell differentiation in

the developing cochlea," *Proceedings of the National Academy of Sciences,* vol. 105, no. 47, pp. 18396-18401, 2008.

[50] W. Pan, Y. Jin, J. Chen, R. J. Rottier, K. Steel and A. E. Kiernan, "Ectopic expression of activated notch or SOX2 reveals similar and unique roles in the development of the sensory cell progenitors in the mammalian inner ear," *Journal of Neuroscience,* vol. 33, no. 41, pp. 16146-16157, 2013.

[51] E. C. Oesterle, S. Campbell, R. R. Taylor, A. Forge and C. R. Hume, "Sox2 and Jagged1 Expression in Normal and Drug-Damaged Adult Mouse Inner Ear," *Journal of the Association for Research in Otolaryngology,* vol. 9, no. 1, pp. 65-89, 2008.

[52] J. Neves, C. Parada, M. Chamizo and F. Giráldez, "Jagged 1 regulates the restriction of Sox2 expression in the developing chicken inner ear: a mechanism for sensory organ specification," *Development,* vol. 138, no. 4, pp. 735-744, 2011.

[53] T. J. Wright and S. L. Mansour, "Fgf3 and Fgf10 are required for mouse otic placode induction," *Development,* vol. 130, no. 15, pp. 3379-3390, 2003.

[54] L. D. Urness, C. N. Paxton, X. Wang, G. C. Schoenwolf and S. L. Mansour, "FGF signaling regulates otic placode induction and refinement by controlling both ectodermal target genes and hindbrain Wnt8a. D," *Developmental Biology,* vol. 340, no. 2, pp. 595-604, 2010.

[55] U. Pirvola, B. Spencer-Dene, L. Xing-Qun, P. Kettunen, I. Thesleff, B. Fritzsch, C. Dickson and J. Ylikoski, "FGF/FGFR-2(IIIb) Signaling Is Essential for Inner Ear Morphogenesis," *Journal of Neuroscience,* vol. 20, no. 16, pp. 6125-6134, 2000.

[56] S. Pauley, T. Wright, U. Pirvola, D. Ornitz, K. Beisel and B. Fritzsch, "Expression and func-tion of FGF10 in mammalian inner ear development," *Developmental Dynamics,* vol. 227, no. 2, pp. 203-215, 2003.

[57] T. Hayashi, C. A. Ray and O. Bermingham-McDonogh, "Fgf20 Is Required for Sensory Epithelial Specification in the Developing Cochlea," *Journal of Neuroscience,* vol. 28, no. 23, pp. 5991-5999, 2008.

[58] S.-H. Huh, J. Jones, M. E. Warchol and D. Onitz, "Differentiation ofthe lateral compartment of the cochlea requires a temporallyrestricted FGF20 signal," *PLoS biology,* vol. 10, no. 1, pp. 1-12, 2012.

[59] W. Chang, Z. Lin, H. Kulessa, J. Hebert, B. L. Hogan and D. K. Wu, "Bmp4 is essential for the formation of the vestibular apparatus that detects angular head movements," *PLoS genetics,* vol. 4, no. 4, pp. 1-14, 2008.

[60] E. R. Andersson, R. Sandberg and U. Lendahl, "Notch signaling: simplicity in design, versatility in function," *Development,* vol. 138, no. 17, pp. 3593-3612, 2011.

[61] J. Murata, K. Ikeda and H. Okano, "Notch signaling and the developing inner ear," in *Notch Signaling in Embryology and Cancer . Advances in Experimental Medicine and Biology*, New York, NY, Springer, 2012, pp. 161-173.

[62] R. Brooker, K. Hozumi and J. Lewis, "Notch ligands with contrasting functions: Jagged1 and Delta1 in the mouse inner ear," *Development,* vol. 133, no. 7, pp. 1277-1286, 2006.

[63] A. E. Kiernan, J. Xu and T. Gridley, "The Notch ligand JAG1 is required for sensory progenitor development in the mammalian inner ear," *PLoS genetics,* vol. 2, no. 1, pp. 27-28, 2006.

[64] N. Yamamoto, W. Chang and M. W. Kelley, "Rbpj regulates development of prosensory cells in the mammalian inner ear," *Developmental Biology,* vol. 353, no. 2, pp. 367-379, 2011.

[65] T. Cai, M. L. Seymour, H. Zhang, F. A. Pereira and A. K. Groves, "Conditional deletion of Atoh1 reveals distinct critical periods for survival and function of hair cells in the organ of Corti," *Journal of Neuroscience,* vol. 33, no. 24, pp. 10110-10122, 2013.

[66] E. C. Driver, L. Sillers, T. M. Coate, M. Rose and M. W. Kelley, "The Atoh1-lineage gives rise to hair cells and supporting cells within the mammalian cochlea," *Developmental Biology,* vol. 376, no. 1, pp. 86-98, 2013.

[67] A. E. Kiernan, "Notch signaling during cell fate determination in the inner ear," *Seminars in Cell & Developmental Biology,* vol. 24, no. 5, pp. 470-479, 2013.

[68] B. E. Jacques, C. Puliglilla, R. M. Weichert, A. Ferrer-Vaquer, A.-K. Hadjantonakis, M. W. Kelley and A. Dabdoub, "A dual function for canonical Wnt/beta-catenin signaling in the developing mammalian cochlea," *Development,* vol. 139, no. 23, pp. 4395-4404, 2012.

[69] B. E. Jacques, W. H. Montgomery IV, P. M. Uribe, A. Yatteau, J. D. Asuncion, G. Resendiz, J. I. Matsui and A. Dabdoub, "The role of Wnt/beta-catenin signaling in proliferation and regeneration of the developing basilar papilla and lateral line," *Developmental Neurobiology,* vol. 74, no. 4, pp. 438-456, 2013.

[70] K. T. Chonko, I. Jahan, J. Stone, M. Wright, T. Fujiyama, M. Hoshino, B. Fritzsch and S. M. Maricich, "Atoh1 directs hair cell differentiation and survival in the late embryonic mouse inner ear," *Developmental Biology,* vol. 381, no. 2, pp. 401-410, 2013.

[71] L. C. Katz and C. J. Shatz, "Synaptic activity and the construction of cortical circuits," *Science,* vol. 274, no. 5290, pp. 1133-1138, 1996.

[72] A. G. Blankenship and M. B. Feller, "Mechanisms underlying spontaneous patterned activity in developing neural circuits," *Nature Reviews Neuroscience,* vol. 11, no. 1, pp. 18-29, 2010.

[73] Y. Ben-Ari, "Developing networks play a similar melody," *Trends in neurosciences,* vol. 24, no. 6, pp. 353-360, 2001.

[74] L. A. Kirkby, G. S. Sack, A. Firl and M. B. Feller, "A role for correlated spontaneous activity in the assembly of neural circuits," *Neuron,* vol. 80, no. 5, pp. 1129-1144, 2013.

[75] M. Geal-Dor, S. Freeman and H. S. Sohmer, "Development of hearing in neonatal rats: air and bone conducted ABR thresholds," *Hearing research,* vol. 69, no. 1-2, pp. 236-242, 1993.

[76] H. C. Wang and D. E. Bergles, "Spontaneous activity in the developing auditory system," *Cell and tissue research,* vol. 361, no. 1, pp. 65-75, 2015.

[77] F. Anselmi, V. H. Hernandez, G. Crispino, A. Seydel, S. Ortolano, S. D. Roper, N. Kessaris, W. Richardson, G. Rickheit, M. A. Filippov, H. Monyer and F. Mammano, "ATP release through connexin hemichannels and gap junction transfer of second messengers propagate Ca2+ signals

across the inner ear," *Proceedings of the National Academy of Sciences,* vol. 105, no. 48, pp. 18770-18775, 2008.

[78] F. Ceriani, T. Pozzan and F. Mammano, "Critical role of ATP-induced ATP release for Ca2+ signaling in nonsensory cell networks of the developing cochlea," *Proceedings of the National Academy of Sciences,* vol. 113, no. 46, pp. E7194-E7201, 2016.

[79] P. Sirko, J. E. Gale and J. F. Ashmore, "Intercellular Ca2+ signalling in the adult mouse cochlea," *The Journal of physiology,* vol. 597, no. 1, pp. 303-317, 2019.

[80] M. P. Abbracchio, G. Burnstock, A. Verkhratsky and H. Zimmermann, "Purinergic signalling in the nervous system: an overview," *Trends in neurosciences,* vol. 32, no. 1, pp. 19-29, 2009.

[81] S. Gorzalka, S. Vittori, R. Volpini, G. Cristalli, I. von Kügelgen and C. E. Müller, "Evidence for the functional expression and pharmacological characterization of adenine receptors in native cells and tissues," *Molecular Pharmacology,* vol. 67, no. 3, pp. 955-964, 2005.

[82] M. Knospe, C. E. Müller, P. Rosa, A. Abdelrahman, v. K. Ivar, D. Thimm and A. C. Schiedel, "The rat adenine receptor: pharmacological characterization and mutagenesis studies to investigate its putative ligand binding site," *Purinergic Signalling,* vol. 9, no. 3, pp. 367-381, 2013.

[83] V. Ralevic and G. Burnstock, "Receptors for purines and pyrimidines," *Pharmacological reviews,* vol. 50, no. 3, pp. 413-492, 1998.

[84] R. A. North, "Molecular physiology of P2X receptors," *Physiological reviews,* vol. 82, no. 4, pp. 1013-1067, 2002.

[85] C. Kaebisch, D. Schipper, P. Babczyk and E. Tobiasch, "The role of purinergic receptors in stem cell differentiation," *Computational and Structural Biotechnology Journal,* vol. 13, pp. 75-84, 2015.

[86] U. Brändle, H. P. Zenner and J. P. Ruppersberg, "Gene expression of P2X-receptors in the developing inner ear of the rat," *Neuroscience letters,* vol. 273, no. 2, pp. 105-108, 1999.

[87] L.-C. Huang, A. F. Ryan, D. A. Cockayne and G. D. Housley, "Developmentally regulated expression of the P2X3 receptor in the mouse cochlea," *Histochemistry and cell biology,* vol. 125, no. 6, pp. 681-692, 2006.

[88] L.-C. Huang, P. R. Thorne, S. M. Vlajkovic and G. D. Housley, "Differential expression of P2Y receptors in the rat cochlea during development," *Purinergic signalling,* vol. 6, no. 2, pp. 231-248, 2010.

[89] N. X. Tritsch, Y.-X. Zhang, G. Ellis-Davies and D. E. Bergles, "ATP induced morphological changes in supporting cells of the developing cochlea," *Purinergic Signalling,* vol. 6, no. 2, pp. 155-166, 2010.

[90] A. Forge, D. J. Jagger, J. J. Kelly and R. R. Taylor, "Connexin30-mediated intercellular communication plays an essential role in epithelial repair in the cochlea," *Journal of Cell Science,* vol. 126, no. 7, pp. 1703-1712, 2013.

[91] F. Mammano, "ATP-dependent intercellular Ca2+ signaling in the developing cochlea: facts, fantasies and perspectives," *Seminars in cell & development biology,* vol. 24, no. 1, pp. 31-39, 2013.

[92] J. H. Lee and D. C. Marcus, "Purinergic signaling in the inner ear," *Hearing research,* vol. 235, no. 1-2, pp. 1-7, 2008.

[93] S. Gonzalez-Gonzalez, "The Role of Purinergic P2X and P2Y Receptors in Hearing Loss," *Journal of Phonetics & Audiology,* vol. 4, no. 1, pp. 2-6, 2018.

[94] M. S. Ford, S. B. Maggirwar, L. P. Rybak, C. Whitworth and V. Ramkumar, "Expression and function of adenosine receptors in the chinchilla cochlea," *Hearing research,* vol. 105, no. 1-2, pp. 130-140, 1997.

[95] G. D. Housley, D. J. Jagger, D. Greenwood, N. P. Raybould, S. G. Salih, L. Järlebark, S. M. Vlajkovic, R. Kanjhan, P. Nikolic, D. J. Muñoz and P. R. Thorne, "Purinergic regulation of sound transduction and auditory neurotransmission," *Audiology and Neurotology,* vol. 7, no. 1, pp. 55-61, 2002.

[96] G. Burnstock, U. Krügel, M. P. Abbrachio and P. Illes, "Purinergic signalling: From normal behaviour to pathological brain function," *Progress in Neurobiology,* vol. 95, no. 2, pp. 229-274, 2011.

[97] F. Ceriani, A. Hendry, J.-Y. Jeng, S. L. Johnson, F. Stephani, J. Olt, M. C. Holley, F. Mammano, J. Engel, C. Kros, D. Simmons and W. Marcotti, "Coordinated calcium signalling in cochlear sensory and non-sensory cells refines afferent innervation of outer hair cells," *The EMBO Journal,* vol. 38, no. 9, p. e99839, 2019.

[98] L. Lagostena and F. Mammano, "Intracellular calcium dynamics and membrane conductance changes evoked by Deiters' cell purinoceptor activation in the organ of Corti," *Cell calcium,* vol. 29, no. 3, pp. 191-198, 2001.

[99] M. E. Warchol, "Sensory regeneration in the vertebrate inner ear: Differences at the levels of cells," *Hearing Research,* vol. 273, no. 1-2, pp. 72-79, March 2011.

[100] H. Suh, W. Deng and F. H. Gage, "Signaling in Adult Neurogenesis," *Annual Review of Cell and Developmental Biology,* no. 25, pp. 253-275, 10 November 2009.

[101] M. Carter and J. Shieh, "Cell Culture Techniques," in *Guide to Research Techniques in Neuroscience*, Cambridge, Academic Press, 2015, pp. 296-309.

[102] K. Y. Kwan, J. Shen and D. P. Corey, "C-MYC Transcriptionally Amplifies SOX2 Target Genes to Regulate Self-Renewal in Multipotent Otic Progenitor Cells," *Stem Cells Report,* vol. 4, no. 1, pp. 47-60, 13 January 2015.

[103] J. Azadeh, Z. Song, A. S. Laureano, A. Toro-Ramos and K. Kwan, "Initiating Differentiation in Immortalized Multipotent Otic Progenitor Cells," *Journal of visualized experiments: JoVE,* vol. 107, no. e53692, 2016.

[104] G. Burnstock and N. Dale, "Purinergic signalling during development and ageing," *Purinergic Signalling,* vol. 11, no. 3, p. 277–305, 2015.

[105] Á. Apáti, T. Berecza and B. Sarkadi, "Calcium signaling in human pluripotent stem cells," *Cell calcium,* vol. 59, no. 2-3, pp. 117-123, 2016.

[106] A. Badura, X. R. Sun, A. Giovannucci, L. A. Lynch and S. S. H. Wang, "Fast calcium sensor proteins for monitoring neural activity," *Neurophotonics,* vol. 1, no. 2, p. 025008, 2014.

[107] R. Y. Tsien, "Fluorescent Indicators of Ion Concentrations," in *Fluorescence Microscopy of Living Cells in Culture Part B. Quantitative Fluorescence Microscopy—Imaging and Spectroscopy*, vol. 30, Academic Press, 1989, pp. 127-156.

[108] R. Buser and A. E. I. Proudfoot, "Calcium Mobilization," in *Methods in Molecular Biology: Chemokine Protocols*, vol. 138, A. E. I. Proudfoot, T. N. Wells and C. Power, Eds., Totowa, NJ, Humana Press Inc., 2000, p. 144.

[109] J. W. Dobrucki and U. Kubitscheck, "Fluorescence Microscopy," in *Fluorescence Microscopy From Principles to Biological Applications*, Second edition ed., U. Kubitscheck, Ed., Weinheim, Wiley-VCH, 2017, pp. 85-132.

[110] A. Minta, J. P. Kao and R. Y. Tsien, "Fluorescent indicators for cytosolic calcium based on rhodamine and fluorescein chromophores," *The Journal of Biological Chemistry,* vol. 264, no. 14, pp. 8171-8178, 1989.

[111] W.-C. Sun, K. R. Gee, D. H. Klaubert and R. P. Haugland, "Synthesis of Fluorinated Fluoresceins," *Journal of Organic Chemistry,* vol. 62, no. 19, pp. 6469-6475, 1997.

[112] K. R. Gee, K. Brown, W.-N. Chen, J. K. Bishop-Stewart, D. R. Gray and I. D. Johnson, "Chemical and physiological characterization of fluo-4 Ca2+- indicator dyes," *Cell Calcium,* vol. 27, no. 2, pp. 97-106, 2000.

[113] V. Prasad, D. Semwogerere and E. R. Weeks, "Confocal microscopy of colloids," *Journal of Physics: Condensed Matter,* vol. 19, no. 11, pp. 113102-113127, 2007.

[114] D. A. Peterson, "Confocal Microscopy," in *The Encyclopedia of Movement Disorders*, Cambridge, Academic Press, 2010, pp. 250-252.

[115] T. J. Fellers and M. W. Davidson, "Olympus Scientific Solutions Americas Corp.," [Online]. Available: https://www.olympus-lifescience.com/en/microscope-resource/primer/techniques/confocal/confocalintro/. [Accessed 08 may 2019].

[116] J. Jonkman and C. M. Brown, "Any way you slice it—a comparison of confocal microscopy techniques," *Journal of Biomolecular Techniques,* vol. 26, no. 2, pp. 54-65, 2015.

[117] P. Uhlén, "Spectral Analysis of Calcium Oscillations," *Sci STKE,* vol. 2004, no. 258, p. pl15, 2004.

[118] N. M. Dayaratne, S. M. Vlajkovic, J. Lipski and P. R. Thorne, "Putative role of border cells in generating spontaneous morphological activity within Kölliker's organ," *Hearing Research,* vol. 330 , no. Part A, pp. 90-97, 2015.

[119] M. Probes, "Fluo Calcium Indicators," Product Information, Eugene, OR , 2011.

[120] V. Piazza, C. D. Ciubotaru, J. E. Gale and F. Mammano, "Purinergic signalling and intercellular Ca2+ wave propagation in the organ of Corti," *Cell calcium,* vol. 41, no. 1, pp. 77-86, 2007.

[121] M. Beltramello, V. Piazza, F. Bukauskas, T. Pozzan and F. Mammano, "Impaired permeability to Ins(1,4,5)P3 in a mutant connexin underlies recessive hereditary deafness," *Nature Cell Biology,* vol. 7, no. 1, pp. 63-69, 2004.

[122] P. M. Dunn and A. Blakeley, "Suramin: a reversible P2-purinoceptor antagonist in the mouse vas deferens," *British Journal of Pharmacology,* vol. 93, no. 2, pp. 243-245, 1988.

[123] C. H. Hoyle, G. E. Knight and G. Burnstock, "Suramin antagonizes responses to P2-purinoceptor agonists and purinergic nerve stimulation in the guinea-pig urinary bladder and taenia coli," *British Journal of Pharmacology,* vol. 99, no. 3, pp. 617-621, 1990.

[124] K. Nakazawa, K. Inoue, K. Fujimori and A. Takanaka, "Effects of ATP antagonists on purinoceptor-operated inward currents in rat phaeochromocytoma cells," *Pflügers Archiv,* vol. 418, no. 3, pp. 214-219, 1991.

[125] J. Franco, L. Scarone and M. A. Comini, "Drugs and Drug Resistance in African and American Trypanosomiasis," *Annual Reports in Medicinal Chemistry,* vol. 51, pp. 97-133, 2018.

[126] R. Bültmann, H. Wittenburg, B. Pause, G. Kurz, P. Nickel and K. Starke, "P2-purinoceptor antagonists: III. Blockade of P2-purinoceptor subtypes and ecto-nucleotidases by compounds related to suramin," *Naunyn-Schmiedeberg's archives of pharmacology,* vol. 354, no. 4, pp. 498-504, 1996.

[127] M. García-Guzmán, F. Soto, J. M. Gómez Hernández, P.-E. Lund and W. Stühmer, "Characterization of recombinant human P2X4 receptor reveals pharmacological differences to the rat homologue," *Molecular pharmacology,* vol. 51, no. 1, pp. 109-118, 1997.

[128] F. Soto, J. M. García-Guzmán, M. Hollman, C. Karschin and W. Stühmer, "P2x4: an ATP-activated ionotropic receptor cloned from rat brain," *Proceedings of the National Academy of Sciences,* vol. 93, no. 8, pp. 3684-3688, 1996.

[129] A. Townsend-Nicholson, B. F. King, S. S. Wildman and G. Burnstock, "Molecular cloning, functional characterization and possible cooperativity between murine P2X4 and P2X4a receptors," *Molecular brain research,* vol. 64, no. 2, pp. 246-254, 1999.

[130] C. A. Jones, I. P. Chessell, J. Simon, E. A. Barnard, K. J. Miller, A. D. Michel and P. P. A. Humphrey, "Functional characterization of the P2X4 receptor orthologues," *British Journal of Pharmacology,* vol. 129, no. 2, pp. 388-394, 2000.

[131] R. A. North, "Molecular physiology of P2X receptors," *Physiological reviews,* vol. 82, no. 4, pp. 1013-1017, 2002.

[132] E. Berekméri, J. Szepesy, L. Köles and T. Zelles, "Purinergic signaling in the organ of Corti: Potential therapeutic targets of sensorineural hearing losses," *Brain Research Bulletin,* vol. 151, pp. 109-118, 2019.

[133] P. Nikolic, G. D. Housley, L. Luo, A. F. Ryan and P. R. Thorne, "Transient expression of P2X1 receptor subunits of ATP-gated ion channels in the developing rat cochlea," *Developmental Brain Research,* vol. 126, no. 2, pp. 173-182, 2001.

[134] L.-C. Huang, D. Greenwood, P. R. Thorne and G. D. Housley, "Developmental regulation of neuron-specific P2X3 receptor expression in the rat cochlea," *Journal of Comparative Neurology,* vol. 484, no. 2, pp. 133-143, 2005.

[135] H.-B. Zhao, N. Yu and C. R. Fleming, "Gap junctional hemichannel mediated ATP release and hearing controls in the inner ear," *Proceedings of the National Academy of Sciences,* vol. 102, no. 51, pp. 18724-18729, 2005.

[136] J. Gale, V. Piazza, C. D. Ciubotaru and F. Mammano, "A mechanism for sensing noise damage in the inner ear," *Current biology,* vol. 14, no. 6, pp. 526-529, 2004.

[137] H. Li, H. Liu and S. Heller, "Pluripotent stem cells from the adult mouse inner ear," *Nature Medicine,* vol. 9, no. 10, pp. 1293-1299, 2003.

[138] K. Oshima, K. Shin, M. Diensthuber, A. W. Peng, A. J. Ricci and S. Heller, "Mechanosensitive Hair Cell-like Cells from Embryonic and Induced Pluripotent Stem Cells," *Cell,* vol. 141, no. 4, pp. 704-716, 2010.

[139] N. Zippel, C. A. Limbach, N. Ratajski, C. L. Urban, A. Pansky, U. Kassack and E. Tobiasch, "Purinergic Receptors Influence the Differentiation of Human Mesenchymal Stem Cells," *Stem Cells and Development,* vol. 21, no. 6, pp. 884-900, 2012.

[140] G. Burnstock and H. Ulrich, "Purinergic signaling in embryonic and stem cell development," *Cellular and Molecular Life Sciences ,* vol. 68, no. 8, pp. 1369-1394, 2011.

[141] P. A. Gottlieb and F. Sachs, "Piezo1: properties of a cation selective mechanical channel," *Channels,* vol. 6, no. 4, pp. 214-219, 2012.

[142] M. M. Pathak, J. L. Nourse, T. Tran, J. Hwe, J. Arulmoli, D. T. T. Le, E. Bernardis, L. A. Flanagan and F. Tombola, "Stretch-activated ion channel Piezo1 directs lineage choice in human neural stem cells," *Proceedings of the National Academy of Sciences,* vol. 111, no. 45, pp. 16148-16153, 2014.

[143] B. Coste, J. Mathur, M. Schmidt, S. R. Early, M. J. Petrus, A. E. Dubin and A. Patapoutian, "Piezo1 and Piezo2 are essential components of distinct mechanically activated cation channels," *Science,* vol. 330, no. 6000, pp. 55-60, 2010.

[144] K. Poole, R. Herget, L. Lapatsina, H.-D. Ngo and G. R. Lewin, "Tuning Piezo ion channels to detect molecular-scale movements relevant for fine touch," *Nature Communications,* vol. 5, no. 3520, 2014.

[145] S. S. Ranade, Z. Qiu, S.-H. Woo, S. Sik Hur, S. E. Murthy, S. M. Cahalan, J. Xu, J. Mathur, M. Bandell, C. Bertrand, Y.-S. J. Li, S. Chien and A. Patapoutian, "Piezo1, a mechanically activated ion channel, is required for vascular development in mice," *Proceedings of the National Academy of Sciences,* vol. 111, no. 28, pp. 10347-10352, 2014.

[146] X. Lu and C. W. Sipe, "Developmental regulation of planar cell polarity and hair-bundle morphogenesis in auditory hair cells: lessons from human and mouse genetics," *Wiley Interdisciplinary Reviews: Developmental Biology,* vol. 5, no. 1, pp. 85-101, 1 January 2016.

[147] G. von Békésy and E. G. Wever, Experiments in Hearing, vol. 8, New York: McGraw-Hill, 1960.

[148] J. Santos-Sacchi, "Asymmetry in voltage-dependent movements of isolated outer hair cells from the organ of Corti," *The Journal of Neuroscience,* vol. 9, no. 8, pp. 2954-2962, 1989.

[149] D. K. Wu and M. W. Kelley, "Molecular mechanisms of inner ear development," *Cold Spring Harbor perspectives in biology,* vol. 4, no. 8, pp. 1-20, 2012.

[150] P. J. J. E. Chen, H. Y. Zoghbi and N. Segil, "The role of Math1 in inner ear development: Uncoupling the establishment of the sensory primordium from hair cell fate determination," *Development,* vol. 129, no. 10, pp. 2495-2505, 2002.

[151] Z. F. Mann and M. W. Kelley, "Development of tonotopy in the auditory periphery," *Hearing Research,* vol. 276, no. 1-2, pp. 12-15, 2011.

[152] M. L. Basch, T. Ohyama, N. Segil and A. Groves, "Canonical Notch signaling is not necessary for prosensory induction in the mouse cochlea: insights from a conditional mutant of RBPjk," *Journal of Neuroscience,* vol. 31, no. 22, pp. 8046-8058, 2011.

[153] J. Li, B. Hou, S. Tumova, K. Muraki, A. Bruns, M. J. Ludlow, A. Sedo, A. J. Hyman, L. McKeown, R. S. Young, N. Y. Yuldasheva, Y. Majeed, L. Wilson, B. Rode, M. A. Bailey and e. a. Kim, "Piezo1 integration of vascular architecture with physiological force," *Nature,* vol. 515, pp. 279-282, 2014.

[154] S. J. Charlton, C. A. Brown, G. A. Weisman, J. T. Turner, L. Erb and M. R. Boarder, "Cloned and transfected P2Y4 receptors: characterization of a suramin and PPADS-insensitive response to UTP," *British Journal of Pharmacology,* vol. 119, no. 7, pp. 1301-1303, 1996.

UNIVERSIDAD DE
GUANAJUATO

León, Gto a 10 de marzo de 2020

Dr. David Yves Ghislain Delepine
Director de la División de Ciencias e Ingenierías
Campus León-UG
Presente

Por este medio me permito informar que he revisado y discutido el documento escrito de la tesis de Maestría de la Lic. Karen Castaño González, del programa de la Maestría en Ciencias Aplicadas de la División de Ciencias e Ingenierías, Campus León, cuyo título es "**Estudio de la generación de estereocilios en precursores de las células ciliadas** ". Manifiesto que estoy de acuerdo con el documento y que la defensa de la tesis se pueda programar.

Agradezco de antemano sus atenciones a la presente y me despido cordinalmente.

Atentamente

"*La Verdad Os Hará Libres*"

Laura E. Castellano
Dra. Laura Edith Castellano Torres
Profesor Investigador

División de Ciencias e Ingenierías
Campus León
Loma del Bosque 103, Col. Lomas del Campestre, León, Gto., CP 37000
Tel. (477) 788 5100 ext. 8534
www.dci.ugto.mx

UNIVERSIDAD DE GUANAJUATO
Campus León
División de Ciencias e Ingenierías

Oficio número: AGV-03-2020-001
Asunto: Carta conformidad
Tesis de Maestría de la estudiante Lic. Karen Castaño González.
León Gto., marzo 10, 2020.

DR. DAVID YVES GHISLAIN DELEPINE
DIRECTOR DE LA DIVISIÓN DE CIENCIAS E INGENIERÍAS
CAMPUS LEÓN
PRESENTE

Estimado Dr. Delepine:

Sirva la presente para hacer de su conocimiento que he revisado el trabajo titulado **"Estudio de la Generación de Estereocilios en Precursores de las Células Ciliadas"** que para obtener el grado de Maestra en Ciencias pone a consideración la **Lic. Karen Castaño González.**

Le comunico que en mi opinión el trabajo reúne las características de nivel y calidad necesarias para una tesis de la Maestría en Ciencias Aplicadas. Asimismo, he discutido con la **Lic. Castaño,** algunos aspectos de su trabajo y le he indicado las correcciones que considero pertinentes, las cuales ha incluido en la versión final del trabajo. De esta manera no tengo objeciones para la presentación del mismo de acuerdo a la reglamentación respectiva.

Agradeciendo la atención prestada a la presente, me despido

A T E N T A M E N T E.
"LA VERDAD OS HARÁ LIBRES"

Dr. Arturo González Vega
Profesor del DIQEB

C.c.p **Karen Castaño González**
C.c.p. Archivo AGV.

DEPARTAMENTO DE INGENIERÍAS QUÍMICA, ELECTRÓNICA Y BIOMÉDICA
Lomas del Bosque #103,
Lomas de Campestre, León Gto.
C.P. 37150
(477) 788 5100 Ext. 8435, Fax. Ext. 8410
www.diqeb.ugto.mx

UNIVERSIDAD DE
GUANAJUATO

Dr. Davis Yves Ghislain Delepine
Director de la División de Ciencias e Ingenierías
Campus León
Universidad de Guanajuato

León, Gto., 20 de febrero del 2020.

Dr. David Delepine:

Por medio de la presente, informo a usted que he leído el manuscrito de tesis del estudiante de la Maestría en Ciencias Aplicadas de la DCI, C. Karen Castaño González, la cual lleva por título: **"Estudio de la generación de estereocilios en precursores de las células ciliadas".** Después de haber realizado mis comentarios, el estudiante realizó las correcciones pertinentes. Por lo anterior doy mi consentimiento para que el **C. Karen Castaño González** defienda de manera oral su tesis de Maestría en la fecha que sus directores de tesis juzguen conveniente.

Sin más por el momento, y agradeciendo las atenciones a la presente, me despido enviando un cordial saludo.

Atentamente:

Dr. Silvia Alejandra López Juárez
Profesor-Investigador

División de Ciencias e Ingenierías
Campus León
Loma del Bosque 103, Col. Lomas del Campestre, León, Gto., CP 37000
Tel. (477) 788 5100 ext. 8493
www.dci.ugto.mx

UNIVERSIDAD DE
GUANAJUATO

León, Gto, a 10 de marzo de 2020

Dr. David Yves Ghislain Delepine
Director de la División de Ciencias e Ingenierías
Campus León, Universidad de Guanajuato

Estimado Dr. Delepine:

Por medio de la presente informo a usted que he leído el manuscrito de tesis de la estudiante de la Maestría en Ciencias Aplicadas de la DCI, C. Karen Castaño González, la cual lleva por título "**Estudio de la Generación de Estereocilios en Precursores de las Células Ciliadas**".

Después de haber realizado mis comentarios, la estudiante realizó las correcciones pertinentes. Por lo anterior doy mi consentimiento para que la **C. Karen Castaño González** defienda de manera oral su tesis de Maestría en la fecha que sus directores de tesis juzguen conveniente.

Sin más por el momento, y agradeciendo la atención a la presente, me despido enviando un cordial saludo

Atentamente

Dr. Luis Carlos Padierna García
Profesor-Investigador

DEPARTAMENTO DE INGENIERÍAS QUÍMICA, ELECTRÓNICA Y BIOMÉDICA
DIVISIÓN DE CIENCIAS E INGENIERÍAS
Loma del Bosque #103, Col. Lomas del Campestre. León, Gto. C.P. 37150
Tel. +52 (477) 7 88 51 00 ext. 8522
lc.padierna@ugto.mx
www.dci.ugto.mx/depingquim